Magnetophotonic intensity effects in hybrid metal-dielectric structures

V. I. Belotelov,[1,2,3] L. E. Kreilkamp,[4] A. N. Kalish,[1,2,3] I. A. Akimov,[4,5] D. A. Bykov,[6] S. Kasture,[7] V. J. Yallapragada,[7] Achanta Venu Gopal,[7] A. M. Grishin,[8] S. I. Khartsev,[8] M. Nur-E-Alam,[9] M. Vasiliev,[9] L. L. Doskolovich,[6] D. R. Yakovlev,[4,5] K. Alameh,[9] A. K. Zvezdin,[2,3] and M. Bayer[4]

[1]*Lomonosov Moscow State University, Leninskie gori, 119991 Moscow, Russia*
[2]*Russian Quantum Center, 143025 Skolkovo, Moscow Region, Russia*
[3]*Prokhorov General Physics Institute, Russian Academy of Sciences, 119991 Moscow, Russia and Moscow Institute of Physics and Technology (State University), Institutskii 9, 117303 Moscow, Russia*
[4]*Experimental Physics 2, TU Dortmund University, 44221 Dortmund, Germany*
[5]*Ioffe Physical-Technical Institute, Russian Academy of Sciences, 194021 St. Petersburg, Russia*
[6]*Image Processing Systems Institute, Russian Academy of Sciences, 443001 Samara, Russia*
[7]*Tata Institute of Fundamental Research, 400005 Mumbai, India*
[8]*Royal Institute of Technology, Kungl Tekniska Hogskolan, 164 40 Stockholm-Kista, Sweden*
[9]*Electron Science Research Institute, Edith Cowan University, 6027 Joondalup, WA, Australia*

(Received 29 October 2013; published 14 January 2014)

The magneto-optical properties of a hybrid metal-dielectric structure consisting of a one-dimensional gold grating on top of a magnetic waveguide layer are studied experimentally and theoretically. It is demonstrated that a magnetic field applied in the longitudinal configuration (in the plane of the magnetic film and perpendicular to the slits in the gold grating) to the metal-dielectric structure modifies the field distribution of the optical modes and thus changes the mode excitation conditions. In the optical far field, this manifests in the alteration of the optical transmittance or reflectance when the structure becomes magnetized. This magneto-optical effect is shown to represent a novel class of effects related to the magnetic-field-induced modification of the Bloch modes of the periodic hybrid structure. That is why we define this effect as "longitudinal magnetophotonic intensity effect" (LMPIE). The LMPIE has two contributions, odd and even in magnetization. While the even LMPIE is maximal for the light polarized perpendicular to the grating slits (TM) and minimal for the orthogonal polarization (TE), the odd LMPIE takes maximum values at some intermediate polarization and vanishes for pure TM and TE polarizations. Two principal modes of the magnetic layer—TM and TE—acquire in the longitudinal magnetic field additional field components and thus turn into quasi-TM and quasi-TE modes, respectively. The largest LMPIE is observed for excitation of the antisymmetrical quasi-TE mode by TM-polarized light. The value of the LMPIE measured for the plasmonic structure with a magnetic film of $Bi_2Dy_1Fe_4Ga_1O_{12}$ composition is about 1% for the even effect and 2% for the odd one. However, the plasmonic structure with a magnetic film with a higher concentration of bismuth ($Bi_{2.97}Er_{0.03}Fe_4Al_{0.5}Ga_{0.5}O_{12}$) gives significantly larger LMPIE: even LMPIE reaches 24% and odd LMPIE is 9%. Enhancement of the magneto-optical figure of merit (defined as the ratio of the specific Faraday angle of a magnetic film to its absorption coefficient) of the magnetic films potentially causes the even LMPIE to exceed 100% as is predicted by calculations. Thus, the nanostructured material described here may be considered as an ultrafast magnetophotonic light valve.

DOI: 10.1103/PhysRevB.89.045118 PACS number(s): 78.66.Bz, 42.25.Fx, 78.20.Ci, 78.20.Ls

I. INTRODUCTION

In the last decade there has been pronounced research interest in the manipulation of optical waves by some external stimuli [1]. The faster optical properties of matter can be modified and the higher the modulation level can be achieved, the more applicable is the method for nanophotonics. In this respect, magneto-optical effects hold great promise since they provide magnetic field control of light at timescales shorter than a fraction of a nanosecond [2]. Two main types of magneto-optical effects can be distinguished: namely, polarization effects related to the magnetic-field-induced modification of the light polarization and intensity effects showing up in changes of the light intensity reflected or transmitted through a magnetized medium [3].

Among the magneto-optical polarization phenomena there are the well-known Faraday, polar Kerr, and longitudinal Kerr effects. On the other hand, the class of the intensity effects is usually associated only with the transverse magneto-optical Kerr effect (TMOKE).

In general, the reflection coefficient of light reflected off a magnetized medium is a function of its magnetization **M**:

$$R(\mathbf{M}) = R_0 + \alpha_i M_i + \beta_{ij} M_i M_j + \cdots , \qquad (1)$$

where $i,j = x,y,z$. The coefficients in the expansion Eq. (1) depend on the medium dielectric constant as well as on the incident light polarization and angle of incidence. In the TMOKE configuration, when a medium is magnetized transversely (**M** lies in the film plane and is perpendicular to the incidence plane) the linear contribution is present ($\alpha_i \neq 0$), and thus the TMOKE is characterized by the relative change of reflected light intensity when the magnetic film is remagnetized ($\mathbf{M} \rightarrow -\mathbf{M}$): $\delta_{\mathrm{TMOKE}} = (R_+ - R_-)/R_0$, where R_+ and R_- are the reflection coefficients for two opposite orientations of the magnetization, and R_0 is the reflectivity for the nonmagnetized case. Typical values of the TMOKE are about $\delta_{\mathrm{TMOKE}} = 10^{-3}$ for Ni and Co in the visible spectral range [4,5]. If the magnetic permeability of a magnetic medium is unity, which is the case for most of the magnetic materials at

visible and near-infrared light, then the TMOKE appears only if the incident light has a p-polarized component (electric field is along the incidence plane). For s-polarized light (electric field is orthogonal to the incidence plane), the TMOKE is absent. Symmetry reasons also demand that the TMOKE exists only for oblique incidence.

Apart from the TMOKE there are some other magneto-optical intensity effects that are much less known mainly due to their smaller magnitudes [3,6], e.g. for the case of the longitudinal magnetization (**M** is in the film plane and is parallel to the incidence plane), the magneto-optical intensity effect is also present. However, this magneto-optical effect differs from the TMOKE in the sense that, for the p and s polarizations of the incident light, it has no first-order **M** contribution, and the quadratic term in Eq. (1) becomes the main one ($\alpha_i = 0, \beta_{ij} \neq 0$).

The even magneto-optical intensity effects in reflection and transmission were experimentally observed in monocrystalline and polycrystalline Fe, Ni, and Co films [7–10]. For bulk crystals, the permittivity tensors usually have more complicated form, and the even magneto-optical intensity effect becomes also sensitive to the orientation of the magnetization and light incidence plane with respect to the crystallographic axes, and its phenomenological description is rather cumbersome [11]. To emphasize this feature, the term "orientational magneto-optical effect" was introduced [12] and comprehensively studied experimentally for metal ferromagnets [6,13–15]. Typical values of the effect for Fe, Ni, and permalloy in the visible and near-infrared spectral ranges are $\delta \sim (0.1 - 1) \times 10^{-3}$ [15].

Recently, many efforts have been made towards elaboration and fabrication of nanostructured materials having outstanding optical properties. Their specially tailored nanostructure allows the existence of different types of modes including propagating and localized surface plasmon-polaritons, waveguide modes, and Fabry-Perot modes [16]. These modes govern the optical response of the nanostructured materials in the far field, leading to resonance dips or peaks in transmission and reflection spectra. It was recently demonstrated that, in such materials, some of the magneto-optical effects also show resonant behavior around the eigenfrequencies of the modes and can be significantly enhanced. The influence of the surface plasmon-polaritons on the magneto-optics was studied in Refs. [17–40]. In particular, a three-orders-of-magnitude increase of TMOKE at the propagating surface plasmon-polariton resonances in a magnetoplasmonic crystal (MPC) was demonstrated [17], with the plasmonic crystal structure being a perforated metal on top of a magnetic dielectric layer. On the other hand, resonances of the Faraday and the polar Kerr effects associated with propagating or localized surface plasmon-polaritons were observed in Refs. [26–29].

Apart from surface plasmon-polaritons, waveguide mode resonances can also lead to enhancement of the magneto-optical effects [41–45]. The excitation of waveguide modes in a two-dimensional (2D) photonic crystal slab consisting of a magnetic material and air holes was shown to be an effective approach to increasing the Faraday rotation [43]. Plasmonic crystal structures of perforated metal covering a magnetic dielectric slab were also shown to provide resonances of the Faraday and Kerr rotation due to excitation of waveguide modes [44,45].

Recently, we have demonstrated that, apart from enhancing established magneto-optical effects, such structures can also be used to give birth to some novel phenomena [46]. Namely, the excitation of the waveguide modes of the structure leads to a magneto-optical intensity effect in the case of a longitudinally magnetized structure. This effect is even in magnetization, and it differs from the orientational effect studied earlier for smooth ferromagnets in the sense that it is due to the excitation of the eigenmodes of the structure. Moreover, the effect is also observed in configurations where the orientational effect vanishes.

In this paper, we present a comprehensive theoretical and experimental study of the recently discovered magneto-optical intensity effect in MPCs. Both the even in magnetization longitudinal intensity effect and its odd counterpart are analyzed. The paper is organized as follows: In Sec. II, we present a theoretical analysis of light intensity modulation by longitudinal magnetic field applied to a smooth or perforated magnetic film. In Sec. III, the experimental and calculation methods used are described. In Sec. IV, the properties of the observed intensity effect and approaches to its enhancement are discussed. Concluding remarks are given in Sec. V.

II. THEORY

In order to understand the origin of the magneto-optical intensity effect in the longitudinally magnetized MPC, we should start from the analysis of the magneto-optical behavior of a bare magnetic dielectric film and of a magnetic film covered with a smooth metal film.

A. The case of a bare magnetic dielectric film

Within the macroscopic theory of magneto-optical phenomena the properties of the magnetically ordered media in the visible and near-infrared light are mainly defined by the $\hat{\varepsilon}$ tensor. In this frequency range, a magnetic-dipole response is very weak, and the magnetic permeability tensor $\hat{\mu}$ is close to a scalar form and can be taken to be unity [3]. In crystals, the dependence of the $\hat{\varepsilon}$ tensor on **M** is given by

$$\varepsilon_{ij} = \varepsilon_{ij}^{(0)} - i e_{ijk} g_k + \delta_{ijkl} M_k M_l, \tag{2}$$

where $g_k = a_{km} M_m$, e_{ijk} is the antisymmetric third-order pseudotensor (the Levi-Civita tensor), and the polar tensors $\varepsilon_{ij}^{(0)}$, a_{km}, and δ_{ijkl} are defined by the crystallographic symmetry of the magnetic material. In the case of an optically isotropic ferromagnet, Eq. (2) is simplified. If the material is magnetized along the x axis, Eq. (2) takes the form

$$\hat{\varepsilon} = \begin{pmatrix} \varepsilon_0 & 0 & 0 \\ 0 & \varepsilon_0 + b & -ig \\ 0 & ig & \varepsilon_0 + b \end{pmatrix}, \tag{3}$$

where $g = a_1 M$, and $b = a_2 M^2$. If light propagates through a bulk ferromagnet in Voigt configuration (wave vector is perpendicular to **M**), its phase velocity depends on the polarization of light, and the effect of linear magnetic birefringence takes place. The refractive index for the light polarized perpendicular to **M** is given by

$$n_\perp = \sqrt{\varepsilon_0 + b - g^2/\varepsilon_0}, \tag{4}$$

while for the light polarized along **M**, the refractive index remains the same as that of the nonmagnetized medium: $n_{||} = \sqrt{\varepsilon_0}$. This means that the reflection coefficient of light at the surface of a ferromagnet magnetized in longitudinal configuration also depends on the magnetization:

$$\begin{aligned} R(M) &= [R_s(\theta) + M^2 R_{s2}(\theta)]\cos^2\psi \\ &\quad + [R_p(\theta) + M^2 R_{p2}(\theta)]\sin^2\psi \\ &\quad + M R_1(\theta)\sin\theta\sin(2\psi) + M^2 R_2(\theta)\sin^2\theta\sin^2(2\psi) \\ &= R_0 + \alpha M + \beta M^2, \end{aligned} \tag{5}$$

where θ is the angle of incidence; $R_s(\theta)$ and $R_p(\theta)$ are reflection coefficients in the absence of magnetization for the s and p polarizations, respectively, given by the conventional Fresnel formulas; $R_1(\theta)$, $R_2(\theta)$, $R_{s2}(\theta)$, and $R_{p2}(\theta)$ are coefficients that define the contributions linear and quadratic in M; and the angle ψ gives the incident linear polarization, being the angle between the electric field vector and the plane of incidence ($\psi = 0^\circ$ for p polarization and $\psi = 90^\circ$ for s polarization; see inset in Fig. 1). It follows from Eq. (5) that the linear term is present only for oblique incidence of light at some intermediate polarization ($0^\circ < \psi < 90^\circ$). For the p or s polarizations, only the quadratic term is present. Additionally, the coefficients in Eq. (5) appear to provide no intensity modification if light is polarized along **M** ($\psi = 0^\circ$) and hits the film normally. The linear term can be determined by measuring the odd signal, defined as

$$\delta_{\text{odd}} = \frac{I(M) - I(-M)}{I(0)} = \frac{2\alpha M}{I(0)}, \tag{6}$$

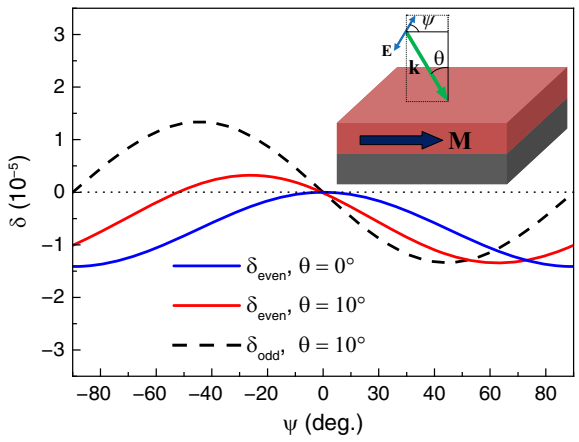

FIG. 1. (Color online) Calculated even and odd longitudinal magneto-optical intensity effects in reflection versus angle of incident light polarization ψ ($\psi = 0^\circ$ and $\psi = \pm 90^\circ$ correspond to p and s polarization, respectively) for incidence angles $\theta = 0^\circ$ and $\theta = 10^\circ$. Light wavelength is 700 nm. The inset shows light incidence configuration. The magnetic film of thickness 1 μm was assumed to be on top of a silica substrate ($\varepsilon = 2.25$). The optical parameters of the magnetic film are chosen to be the following: $\varepsilon_0 = 5.34 + 0.012i$, $g = (2.3 + 0.2i) \times 10^{-3}$, and $b = 3 \times 10^{-5}$, corresponding to a bismuth-substituted iron garnet film at the near-infrared spectral range. Calculations were made using the rigorous coupled-waves analysis (see Sec. III.A).

where I denotes the reflectance R. On the other hand, the quadratic contribution in M comes from the even signal, defined as

$$\delta_{\text{even}} = \frac{I(M) - I(0)}{I(0)} = \frac{\alpha M + \beta M^2}{I(0)}. \tag{7}$$

Equation (5) is valid for a single interface between the nonmagnetized and longitudinally magnetized media. It must be modified for a magnetic film of finite thickness if the reflection from the bottom surface of the magnetic film is not negligible and interference of forward and backward waves inside the magnetic film takes place. Nevertheless, the qualitative behavior remains the same. Similar reasoning is also valid for transmitted light; however, in this case, I in Eqs. (6) and (7) stands for transmittance T.

The typical polarization angle dependences of the even and odd longitudinal intensity magneto-optical effects are shown in Fig. 1. The magnitudes of both effects are of the order of 10^{-5}.

B. The case of a magnetic film covered with a smooth metal film

We assume that the magnetic film rests on a nonmagnetic substrate of lower refractive index so that waveguide modes in the magnetic film exist. In the following consideration, only one magneto-optical parameter g is used to simplify the analysis. Nevertheless, the contribution of the second-order parameter b is also taken into account. Since g and b are linear and quadratic in magnetization, respectively, b can be formally expressed via g as $b = ag^2$. Therefore, b is implicitly included in the forthcoming analysis.

The electromagnetic field of a waveguide mode with the wavenumber κ in the magnetic layer is described by a superposition of four plane waves [the coordinate axes are chosen similar to those shown in Fig. 2(a)]:

$$\begin{aligned} \mathbf{E}(x,z) = \big[&K_1\mathbf{e}_2^{(a+)}\exp(i\gamma_a z) + K_2\mathbf{e}_2^{(a-)}\exp(-i\gamma_a z) \\ &+ K_3\mathbf{e}_2^{(b+)}\exp(i\gamma_b z) + K_4\mathbf{e}_2^{(b-)}\exp(-i\gamma_b z)\big] \\ &\times \exp[i(\kappa x - \omega t)], \end{aligned} \tag{8}$$

where ω is the angular frequency, and $\mathbf{e}_2^{(l\pm)}$ is a unit electric field vector for a plane wave of certain polarization which is denoted by a or b, and κ and γ_l are the components of the wave vector: $\mathbf{k}^{(l\pm)} = \{\kappa; 0; \pm\gamma_l\}$. Both $\mathbf{e}_2^{(l)}$ and γ_l are found from the Fresnel equation

$$[n^{(l)}]^2\mathbf{e}_2^{(l)} - \mathbf{n}^{(l)}\big[\mathbf{n}^{(l)}\mathbf{e}_2^{(l)}\big] = \hat{\varepsilon}\mathbf{e}_2^{(l)}, \tag{9}$$

where $\mathbf{n}^{(l)} = c\omega^{-1}\mathbf{k}^{(l)}$ is the refraction vector, and c is the speed of light in vacuum. Equation (9) provides two solutions, that are γ_a and γ_b, for either positive or negative $n_z^{(l)}$. Within the linear-in-g approximation, these solutions can be represented as $\gamma_{a,b} = \gamma_2 \pm \Delta\gamma$, where $\gamma_2 = (\varepsilon_0\omega^2c^{-2} - \kappa^2)^{1/2}$ and $\Delta\gamma = 0.5g\varepsilon_0^{-1/2}\kappa\omega(\gamma_2 c)^{-1}$.

In isotropic surrounding media, the components of the electromagnetic field of the modes can be divided into two groups: the transverse electric (TE) components, H_x, E_y, and H_z, and the transverse magnetic (TM) ones, E_x, H_y, and E_z. The electromagnetic field contains both TE and TM

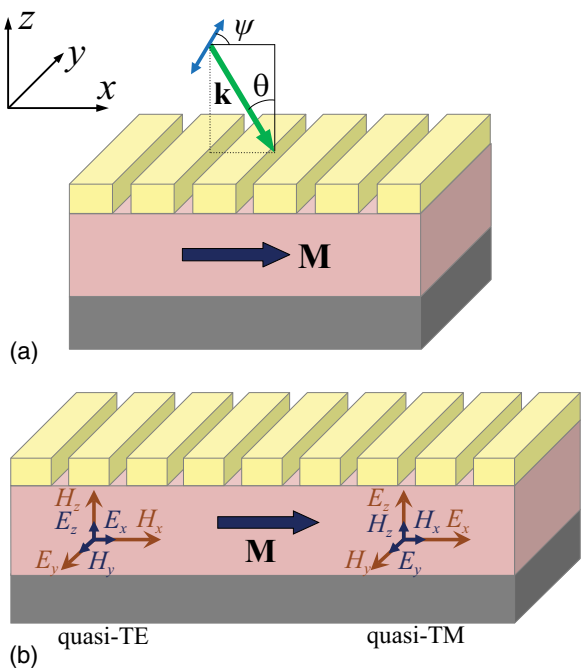

FIG. 2. (Color online) (a) Schematic of the MPC and configuration of light incidence. (b) Quasi-TE and quasi-TM modes of the MPC. The long brown arrows represent principal components of the electromagnetic field, and the short blue arrows represent components induced by magnetization.

components

$$\mathbf{E}(x,z) = \left[A_j \mathbf{e}_j^{(TE)} + B_j \mathbf{e}_j^{(TM)}\right] \exp(-\gamma_j |z|) \times \exp[i(\kappa x - \omega t)], \tag{10}$$

where $j = 1$ for the metal and $j = 3$ for the substrate, $\gamma_j = (\kappa^2 - \varepsilon_j \omega^2 c^{-2})^{1/2}$, ε_j is the corresponding dielectric constant, and $\mathbf{e}_j^{(l)}$ is the unit electric field vector for the polarization denoted by (l): $\mathbf{e}_j^{(TM)} = \frac{1}{\sqrt{|E_x|^2+|E_z|^2}}(E_x, 0, E_z)$ and $\mathbf{e}_j^{(TE)} = \frac{1}{|E_y|}(0, E_y, 0)$.

The boundary conditions for the **E** and **H** vectors at the metal/magnetic-dielectric and magnetic-dielectric/substrate interfaces form a homogeneous linear algebraic set of equations for the coefficients A_i, B_i, and K_i in Eqs. (8) and (10). The condition for the existence of a nontrivial solution of these simultaneous equations leads to the following dispersion equation:

$$\Phi(\kappa,\omega) = g^2 \Psi(\kappa,\omega), \tag{11}$$

where

$$\Phi(\kappa,\omega) = \left[\gamma_2(\gamma_1+\gamma_3) + \left(\gamma_1\gamma_3 - \gamma_2^2\right)\tan(\gamma_2 h_m)\right] \times \left[\frac{\gamma_2}{\varepsilon_0}\left(\frac{\gamma_1}{\varepsilon_1} + \frac{\gamma_3}{\varepsilon_3}\right) + \left(\frac{\gamma_1\gamma_3}{\varepsilon_1\varepsilon_3} - \frac{\gamma_2^2}{\varepsilon_0^2}\right)\tan(\gamma_2 h_m)\right] = \Phi_1(\kappa,\omega)\Phi_2(\kappa,\omega), \tag{12}$$

h_m is the magnetic layer thickness, and $\Psi(\kappa,\omega)$ is determined by the optical and geometrical parameters of the structure (the expression for $\Psi(\kappa,\omega)$ is not presented because of its complexity). Excluding some specific cases when $\frac{\partial\Phi}{\partial\omega}(\kappa,\omega_0) = 0$, where ω_0 is the mode frequency for the demagnetized system so that $\Phi(\kappa,\omega_0) = 0$, and taking into account the smallness of g, the application of a Taylor expansion to Eq. (11) shows that the magnetic contribution to the wavenumber is quadratic in gyration and, consequently in M,

$$\frac{\partial\Phi}{\partial\omega}(\kappa,\omega_0)(\omega-\omega_0) = g^2\Psi(\kappa,\omega_0), \tag{13}$$

so that

$$\omega(\kappa) = \omega_0(\kappa)(1+\zeta g^2), \tag{14}$$

where $\zeta = \Psi(\kappa,\omega_0)\omega_0^{-1}[\frac{\partial\Phi}{\partial\omega}(\kappa,\omega_0)]^{-1}$.

It follows from Eqs. (12)–(14) that there are two families of modes, determined by the equations $\Phi_1(\kappa,\omega_0) = 0$ and $\Phi_2(\kappa,\omega_0) = 0$, respectively. The corresponding dispersion laws given by Eq. (14) appear to be close to that of the conventional TE and TM modes for nonmagnetic waveguides, so we designate these families as quasi-TE and the quasi-TM modes.

Substituting the coefficients A_i, B_i, and K_i found from the boundary conditions into Eqs. (9) and (10) reveals that all six components of the electromagnetic field are nonzero. For a demagnetized structure, the components E_x, H_y, and E_z of the quasi-TE modes vanish, as do the components H_x, E_y, and H_z for the quasi-TM modes. This fact explains the modes designation. Within the linear-in-g approximation, these components are proportional to M, in particular, for the quasi-TM modes

$$E_y^{TM}(x,z) = gF(\kappa,z)\,H_y^{TM}(x,z), \tag{15}$$

and for the quasi-TE modes

$$H_y^{TE}(x,z) = gG(\kappa,z)\,E_y^{TE}(x,z), \tag{16}$$

whereas the gyration contribution to the principal components (E_x, H_y, and E_z for the quasi-TM modes and H_x, E_y, and H_z for the quasi-TE modes) is only quadratic. The functions $F(\kappa,z)$ and $G(\kappa,z)$ are presented in Appendix A. It is important to note here that these functions are odd in κ. Equations (15) and (16) remain valid in the surrounding media as well, with functions $F_i(\kappa)$ and $G_i(\kappa)$ now independent of z.

C. Waveguide modes in the case of a magnetic film covered with a metal grating (MPC)

If a magnetic film is covered with a one-dimensional metal grating, see Fig. 2(a), the optical properties of the structure change significantly. The grating periodicity plays a twofold role. On one hand, it allows excitation of the eigenmodes of the structure, which is not possible for smooth films without prism devices. On the other hand, the metal grating modifies the eigenmodes leading to their plasmonic and Bloch wave characters. Moreover, the periodic structuring causes mode leakage into the surrounding media. The optical far-field properties also get altered since the eigenmodes lead to resonance lines with nonsymmetric Fano shape in the transmittance T and reflectance R spectra [47]. Consequently, the analysis of the modes of the considered metal-dielectric structure is essential to understand and predict its magneto-optical behavior.

In this case, the waveguide modes have the form of Bloch waves

$$\mathbf{E}(x,z) = \mathbf{U}(\kappa,x,z)\exp(i\kappa x), \tag{17}$$

where κ is the quasiwavenumber and $\mathbf{U}(\kappa,x,z)$ is a periodic function of x, and thus, it can be expanded as a Fourier series

$$\mathbf{E}(x,z) = \sum_m \mathbf{U}_m(\kappa,z)\exp\left[i\left(\kappa + \frac{2\pi}{d}m\right)x\right], \tag{18}$$

where m is an integer, and d is the grating period.

The influence of slits can be estimated through perturbation theory [48,49]. We assume that the width of the slits is rather small in comparison to the eigenmode wavelength. In the zeroth approximation the dispersion law is given by the empty lattice approximation

$$\omega^{(0)}(\kappa) = \bar{\omega}(\pm\kappa + 2\pi m/d), \tag{19}$$

where $\bar{\omega}(\bar{\kappa})$ is the dispersion law for the nonperforated structure, so that it is defined by Eq. (14) with $\bar{\omega}$ substituted for ω. Equation (19) provides a discrete set of frequencies for each quasiwavenumber κ.

For a given frequency ω, the amplitudes of the Bloch waves in the zeroth order approximation have the form

$$\mathbf{U}_m(\kappa,z) = A\delta_{mm_0}\mathbf{e}(\pm\kappa + 2\pi m/d,z), \tag{20}$$

where A is the normalization constant, $\mathbf{e}(\bar{\kappa},z)$ is the unit polarization vector of the mode with the wavenumber $\bar{\kappa}$ in the absence of the slits, δ_{mm_0} is the Kronecker symbol, and m_0 is taken from the condition $\omega = \bar{\omega}(\pm\kappa + 2\pi m_0/d)$. In particular, this implies that the polarization properties of the modes are similar to those of the smooth metal film described in the previous section, i.e. there are quasi-TE and quasi-TM modes, as shown in Fig. 2(b).

At the Γ point of the Brillouin zone ($\kappa = 0$) the dispersion curves of the modes propagating along and opposite to the x axis intersect, and the interaction between the modes leads to anticrossing and formation of bandgaps while the modes of the perforated system in the zeroth order approximation on the slits width have the form

$$|\psi^{(0)}\rangle = C_1|\psi_+^{(0)}\rangle + C_2|\psi_-^{(0)}\rangle, \tag{21}$$

where $|\psi_+^{(0)}\rangle$ and $|\psi_-^{(0)}\rangle$ denote modes propagating along and opposite to the x axis, respectively. Here, we use the Dirac notation for the generalized description of the modes. The representations of these generalized vectors can be different; for example, in the scattering matrix analysis, it is convenient to deal with vectors consisting of electric and magnetic field amplitudes for the spatial harmonics in the surrounding media [50]. Within this subsection of the paper, the mode vector $|\psi_i\rangle$ denotes the electric field distribution inside the structure.

The amplitudes C_1 and C_2 as well as the corrected frequencies $\omega^{(1)}$ are found from the following eigenvalue problem [49,51]:

$$\begin{pmatrix} \omega^{(0)} + V_{11} & V_{12} \\ V_{21} & \omega^{(0)} + V_{22} \end{pmatrix}\begin{pmatrix} C_1 \\ C_2 \end{pmatrix} = \omega^{(1)}\begin{pmatrix} C_1 \\ C_2 \end{pmatrix}. \tag{22}$$

The elements of the interaction matrix V_{ij} can be estimated using perturbation theory for the Maxwell's equations [48,51]

$$V_{ij} \approx \langle\psi_i^{(0)}|\mathbf{V}(\Delta\varepsilon)|\psi_j^{(0)}\rangle, \tag{23}$$

where $\mathbf{V}(\Delta\varepsilon)$ is an operator depending on the local perturbation of the dielectric constant $\Delta\varepsilon$ caused by the slits. Note that all the quantities V_{ij} as well as frequencies $\omega^{(0)}$ and $\omega^{(1)}$ have imaginary parts arising from both absorptive and radiative losses.

Let us take $x = 0$ at the center of a slit. The phases of the modes $|\psi_+^{(0)}\rangle$ and $|\psi_-^{(0)}\rangle$ can be chosen in such a way that the principal components are in-phase for these modes at $x = 0$, namely:

$$\begin{aligned} E_{y\pm}^{TE} &\propto A(z)\exp\left(\pm i\frac{2\pi}{d}m_0 x\right), \\ H_{y\pm}^{TM} &\propto B(z)\exp\left(\pm i\frac{2\pi}{d}m_0 x\right), \end{aligned} \tag{24}$$

and the other components are easily found from the Maxwell's equations and Eqs. (15) and (16).

Since the magnetization is an axial vector, the structure under the operation $x \to -x$ transforms into itself, while the modes $|\psi_+^{(0)}\rangle$ and $|\psi_-^{(0)}\rangle$ transform into $|\psi_-^{(0)}\rangle$ and $|\psi_+^{(0)}\rangle$, respectively. Therefore, the elements of the interaction matrix satisfy the relations $V_{11} = V_{22}$ and $V_{12} = V_{21}$. Then, solving Eq. (22) yields two eigenmodes, namely, the symmetric mode $|\psi_s^{(0)}\rangle = \frac{1}{\sqrt{2}}(|\psi_+^{(0)}\rangle + |\psi_-^{(0)}\rangle)$ with the complex frequency $\omega_s^{(1)} = \omega^{(0)} + V_{11} + V_{12}$ and the antisymmetric mode $|\psi_a^{(0)}\rangle = \frac{1}{\sqrt{2}}(|\psi_+^{(0)}\rangle - |\psi_-^{(0)}\rangle)$ with the complex frequency $\omega_a^{(1)} = \omega^{(0)} + V_{11} - V_{12}$.

The operator $\mathbf{V}(\Delta\varepsilon)$ is a multiplicative one (see Ref. [48]), so that the electromagnetic field components enter Eq. (23) only in second power. According to Eqs. (15) and (16), this implies that Eq. (23) does not contain a linear-in-g term; hence, in the presence of the slits, the magneto-optical contribution to mode dispersion remains quadratic, as in Eq. (14).

Let us consider the symmetric quasi-TE mode. It follows from Eq. (24) that its electric E_{ys} and magnetic H_{xs} components are even in x

$$E_{ys}^{TE} \propto E_{y+}^{TE} + E_{y-}^{TE} \propto A(z)\cos\left(\frac{2\pi}{d}m_0 x\right). \tag{25}$$

Since for a fixed z value, $H_{x\pm} \propto E_{y\pm}$ and $H_{z\pm} \propto \kappa E_{y\pm} \propto \pm E_{y\pm}$, the H_{xs}^{TE} and H_{zs}^{TE} components are even and odd in x, respectively.

Taking into account that $G(\kappa,z)$ in Eq. (16) is odd in κ, the admixed components of the symmetric quasi-TE-mode are linear in magnetization, H_y and E_x are odd in x, and E_z is even in x, that is

$$\begin{aligned} H_{ys}^{TE} &\propto gG\left(\frac{2\pi m_0}{d},z\right)A\exp\left(i\frac{2\pi}{d}m_0 x\right) \\ &\quad + gG\left(-\frac{2\pi m_0}{d},z\right)A\exp\left(-i\frac{2\pi}{d}m_0 x\right) \\ &\propto gG\left(\frac{2\pi m_0}{d},z\right)A\sin\left(\frac{2\pi}{d}m_0 x\right). \end{aligned} \tag{26}$$

Similar properties can be easily obtained for all types of modes.

TABLE I. Spatial parity properties of the MPC modes.

Modes	Principal components		Admixed components, linear in magnetization	
	Even in x	Odd in x	Even in x	Odd in x
Symmetric quasi-TE	E_y, H_x	H_z	E_z	H_y, E_x
Antisymmetric quasi-TE	H_z	E_y, H_x	H_y, E_x	E_z
Symmetric quasi-TM	H_y, E_x	E_z	H_z	E_y, H_x
Antisymmetric quasi-TM	E_z	H_y, E_x	E_y, H_x	H_z

Strictly speaking, Eqs. (25) and (26) are valid only in zeroth order approximation, i.e. for vanishing slit width. However, the symmetry properties of the modes remain the same irrespective of the slit width (the proof is given in Appendix B).

The summary of the spatial parity properties of different modes of the MPC is given in Table I.

D. Origin of the even and odd magneto-optical intensity effects

The eigenmodes of the structure can be excited along the x axis by an incident wave with wave vector component $k_x^{(i)}$ if momentum conservation is fulfilled, $k_x^{(i)} = \kappa + 2\pi m/d$, where m is an integer. In addition, the incident light wave must have proper polarization matching with the electromagnetic field of the mode, i.e. the incident wave should contain at least one field component that is present also in the eigenmode.

One more condition for the eigenmodes excitation is imposed by the spatial symmetry reasoning. For example, at the normal incidence, the plane wave polarized at some angle ψ possesses in-plane electromagnetic field components (E_x, E_y, H_x, and H_y) that are independent of x and y, and hence they have even-in-x parity. This implies that such incident wave can excite only those modes for which in-plane components present in this wave have even-in-x parity. In particular, in the absence of magnetization, it is evident from Table I that, at the normal incidence, only symmetric modes can be excited.

The magnetization-induced changes in the waveguide mode properties lead to modification of the far-field response. It can be shown via the scattering matrix analysis that the far-field amplitude in the spectral vicinity of a resonance caused by an eigenmode excitation has the form [18,51]

$$A(\omega) = \frac{a_r}{\omega - \omega_r} + a_{nr}, \tag{27}$$

where ω_r is the complex pole of the scattering matrix, while a_r and a_{nr} are amplitudes of the resonant and nonresonant terms, respectively. In terms of physics, this is the complex frequency of an eigenmode given by Eq. (14). The first term in Eq. (27) is related to resonant excitation of a mode, and the second term is related to direct nonresonant scattering without interaction with the MPC modes.

The electromagnetic field distribution has the following structure. A Rayleigh expansion can be applied to the near-field distribution in the light incidence medium [52,53]

$$\mathbf{E}(\mathbf{r}) = \mathbf{E}^{(i)} \exp\left[ik_x x - ik_{z0}^{(i)} z\right] + \sum_m \mathbf{E}_m^{(r)} \exp\left[ik_x x + i\frac{2\pi}{d} mx + ik_{zm}^{(i)} z\right], \tag{28}$$

and in the substrate

$$\mathbf{E}(\mathbf{r}) = \sum_m \mathbf{E}_m^{(t)} \exp\left[ik_x x + i\frac{2\pi}{d} mx - ik_{zm}^{(s)} z\right]. \tag{29}$$

Here, k_x is the in-plane component of the incident wave vector, and $k_{zm}^{(i,s)} = \sqrt{\varepsilon_{i,s}\omega^2 c^{-2} - (k_x + 2\pi m d^{-1})^2}$, $\varepsilon_{i,s}$ is the dielectric constant of the light incidence medium or substrate. The field inside the structure can be expanded in a Bloch-Fourier series

$$\mathbf{E}(\mathbf{r}) = \sum_m \mathbf{E}_m(z) \exp\left(ik_x x + i\frac{2\pi}{d} mx\right). \tag{30}$$

The electromagnetic field of the incident wave will be denoted by $|\psi^{(\mathrm{in})}\rangle$. Physically, it refers to the first term in Eq. (28) and contains only the zeroth spatial harmonic ($m = 0$). The scattered field will be denoted by $|\psi^{(\mathrm{out})}\rangle$ and corresponds to the second term in Eq. (28) and the whole field in Eq. (29). The field inside the structure [Eq. (30)] is composed of both $|\psi^{(\mathrm{in})}\rangle$ and $|\psi^{(\mathrm{out})}\rangle$. The incident and scattered waves are connected via the scattering operator $\mathbf{S}$ of the MPC [50]

$$|\psi^{(\mathrm{out})}\rangle = \mathbf{S}(\omega,\kappa)\,|\psi^{(\mathrm{in})}\rangle. \tag{31}$$

If an eigenmode is excited in the structure, its electromagnetic field will be denoted by $|\psi^{(\mathrm{eig})}\rangle$, so it is a resonant part of $|\psi^{(\mathrm{out})}\rangle$. The electromagnetic field of a mode $|\psi^{(\mathrm{eig})}\rangle$ inside the structure is given by Eq. (18). The total field inside the structure given by Eq. (30) contains the field of a mode and the field of the direct scattering without mode excitation.

The zeroth-order reflection and transmission coefficients of the structure refer to the zeroth spatial harmonic ($m = 0$) of the fields described by Eqs. (28) and (29). The amplitudes of the zeroth harmonics [see Eq. (28)] are given by

$$A_{TE}^{(r,t)} = E_{y0}^{(r,t)}, \quad A_{TM}^{(r,t)} = \frac{E_{x0}^{(r,t)}}{\cos\theta_{r,t}} = \frac{H_{y0}^{(r,t)}}{\sqrt{\varepsilon_{i,s}}}, \tag{32}$$

where θ_r and θ_t are the angles of reflection and transmission, respectively. The corresponding far-field intensity is given by

$$I(\omega) \propto |A_{TM}(\omega)|^2 + |A_{TE}(\omega)|^2. \tag{33}$$

The field of the incident wave can be decomposed into two terms:

$$|\psi^{(\mathrm{in})}\rangle = \left|\psi_{\mathrm{res}}^{(\mathrm{in})}\right\rangle + \left|\psi_{nr}^{(\mathrm{in})}\right\rangle, \tag{34}$$

where $|\psi_{\mathrm{res}}^{(\mathrm{in})}\rangle$ is the resonant term responsible for the excitation of an eigenmode, and $|\psi_{nr}^{(\mathrm{in})}\rangle$ is orthogonal to it (i.e. it is the nonresonant term). Consequently, $|\psi_{\mathrm{res}}^{(\mathrm{in})}\rangle \propto \mathbf{S}^{-1}(\omega,\kappa)\,|\psi^{(\mathrm{eig})}\rangle$, where $|\psi^{(\mathrm{eig})}\rangle$ is one of the eigenmodes considered above,

and $\mathbf{S}(\omega,\kappa)$ is the scattering matrix of the structure [35]. It is well known that the eigenmodes are the solutions of the equation $\mathbf{S}^{-1}(\omega_0,\kappa)|\psi^{(\mathrm{eig})}\rangle = 0$, where ω_0 is the complex pole of the scattering matrix for given κ. This implies that, for real frequencies, $\mathbf{S}^{-1}(\omega,\kappa)|\psi^{(\mathrm{eig})}\rangle$ is nonzero.

Assumption. For the qualitative analysis, it is assumed that the coefficients a_r and a_{nr} in Eq. (27) are proportional to the amplitudes of the resonant and nonresonant terms in Eq. (34), respectively, so that $a_r \propto \langle\psi^{(\mathrm{in})}|\mathbf{S}^{-1}(\omega,\kappa)|\psi^{(\mathrm{eig})}\rangle$, $a_{nr} \propto [\langle\psi^{(\mathrm{in})}|\psi^{(\mathrm{in})}\rangle - |\langle\psi^{(\mathrm{in})}|\mathbf{S}^{-1}(\omega,\kappa)|\psi^{(\mathrm{eig})}\rangle|^2]^{1/2}$. This approximation is made only qualitatively on the basis of the Breit-Wigner formula for the scattering matrix [54].

Notation. For the analysis of the far-field response of the MPC, the polarization and symmetry properties of the eigenmodes and of the incident wave become essential. The electromagnetic field contains TE and TM components which can be characterized by E_y and H_y, respectively. For the sake of convenience, further on in this subsection, we will use the following notation: if a field $|\psi\rangle$ has a symmetric (antisymmetric) E_y component of amplitude $A(x,z)$ and a symmetric (antisymmetric) H_y component of amplitude $B(x,z)$, it will be written as

$$|\psi\rangle = \begin{pmatrix} A_{s(a)} \\ B_{s(a)} \end{pmatrix}. \tag{35}$$

With the assumption that $g \ll 1$ any linear-in-g quantity is denoted $O(g)$ and any quantity independent of g is denoted $O(1)$. The quantities that have third or higher orders in g are neglected.

Having made the necessary assumptions and introduced the notation, we now present the analysis of the far-field response of the magnetized MPC. The four types of eigenmodes shown in Table I can be present in the structure. Moreover, the cases of normal and oblique incidence must be treated separately because their symmetry properties are different. Further, we consider all possible cases, referring to either TM or TE polarization of the incident light.

Case I. Normal incidence, the incident wave is TM polarized, and its frequency is close to that of the antisymmetric quasi-TE mode. For normal incidence ($k_x = 0$), the field of the incident wave is always symmetric, so that

$$|\psi^{(\mathrm{in})}\rangle = \begin{pmatrix} 0 \\ 1_s \end{pmatrix}. \tag{36}$$

The antisymmetric quasi-TE mode possesses a symmetric H_y component that is linear in g, while its E_y component is antisymmetric and does not have the linear-in-g contribution (see Table I). So, the incident wave decomposition Eq. (33) takes the form

$$|\psi^{(\mathrm{in})}\rangle = c_1 \begin{Bmatrix} [1+O(g^2)]_a \\ O(g)_s \end{Bmatrix}_{\mathrm{res}} + c_2 \begin{Bmatrix} [1+O(g^2)]_a \\ O(g)_s \end{Bmatrix}_{nr} + c_3 \begin{Bmatrix} O(g)_a \\ [1+O(g^2)]_s \end{Bmatrix}_{nr}. \tag{37}$$

The first term in Eq. (37) comes directly from the properties of the antisymmetric quasi-TE mode. According to Eq. (26), the quantity $O(g)_s$ is related to $G(\kappa,z)$. The other quantities $O(g)$ arise because of the $O(g)_s$ in the first term, so they are also related to $G(\kappa,z)$. The second and the third terms in Eq. (37) are the parts of $|\psi^{(\mathrm{in})}_{nr}\rangle$ with the polarizations the same as for the mode and orthogonal to it, respectively. Thus, the second and the third terms are orthogonal to each other.

As the first and the second terms have the same polarization, it can be assumed that c_1 and c_2 have the same dependence on g. The coefficients c_i are found from comparing the right parts of Eqs. (36) and (37) via Cramer's rule

$$c_1 \sim c_2 \sim \frac{\begin{vmatrix} 0 & O(g) \\ 1 & [1+O(g^2)] \end{vmatrix}}{\begin{vmatrix} [1+O(g^2)] & O(g) \\ O(g) & [1+O(g^2)] \end{vmatrix}} = O(g),$$
$$c_3 \sim \frac{\begin{vmatrix} [1+O(g^2)] & 0 \\ O(g) & 1 \end{vmatrix}}{\begin{vmatrix} [1+O(g^2)] & O(g) \\ O(g) & [1+O(g^2)] \end{vmatrix}} = 1+O(g^2), \tag{38}$$

therefore

$$|\psi^{(\mathrm{in})}\rangle = \begin{pmatrix} 0 \\ 1_s \end{pmatrix} = O(g) \begin{Bmatrix} [1+O(g^2)]_a \\ O(g)_s \end{Bmatrix}_{\mathrm{res}} + O(g) \begin{Bmatrix} [1+O(g^2)]_a \\ O(g)_s \end{Bmatrix}_{nr} + [O(1)+O(g^2)] \begin{Bmatrix} O(g)_a \\ [1+O(g^2)]_s \end{Bmatrix}_{nr}. \tag{39}$$

According to our assumption related to a_r and a_{nr} (see the paragraph Assumption above), the first term of Eq. (39) produces the resonant far-field response with the order in g of $O(g)\cdot O(g) = O(g^2)$ for the TM component. The second term is the nonresonant term with a similar order in g as the first term, and the third term has the TM component amplitude $[O(1)+O(g^2)]^2 \approx [O(1)+O(g^2)]$. Thus, from Eq. (28), for the amplitude of the TM component in the far-field, we obtain

$$A_{TM}(\omega) = \frac{O(g)\cdot O(g)}{\omega-\omega_0+O(g^2)} + O(g)\cdot O(g) + O(1) + O(g^2) = \frac{O(g^2)}{\omega-\omega_0} + \frac{O(g^2)}{(\omega-\omega_0)^2} + O(1) + O(g^2). \tag{40}$$

Here, Eq. (14) is taken into account so that the complex pole of the scattering matrix has a quadratic-in-g contribution. At the same time, as it is seen from Eq. (37), the E_y component of the electromagnetic field is antisymmetric (i.e. it is odd in x); hence, it does not contain the zeroth spatial harmonic [$E_{y0} = 0$, see Eqs. (28)–(30)]. Therefore, $A_{TE} = 0$, and according to Eq. (33), the far-field intensity is determined only by A_{TM}.

We now come to the conclusion that the far-field response exhibits a magnetization-induced resonance feature that has even parity in M. Therefore, using Eq. (40) with Eq. (33) and Eq. (7), one can determine the even-in-magnetization signal

$$\delta_{\mathrm{even}}(\omega) = \frac{I(g,\omega) - I(0,\omega)}{I(0,\omega)} \propto O(g^2)\mathrm{Re}\left[\frac{O(1)}{\omega-\omega_0} + \frac{O(1)}{(\omega-\omega_0)^2} + O(1)\right]. \tag{41}$$

This function becomes dominant through the resonance in the vicinity of the antisymmetric quasi-TE mode. Note that, in a nonmagnetic structure, this mode is "dark", i.e. it cannot be excited, as was shown above. The origin of the effect is the coupling of the TE and TM field components of the modes in the magnetized structure (see Table I) and consequential excitation of modes that are not excited in the nonmagnetized case. According to Eq. (41), $\delta_{\text{even}}(\omega)$ contains both resonance and nonresonance terms, so it is expected to have a Fano-type spectral line shape. The latter is characterized by a peak followed immediately by a dip, or vice versa.

Case II. Normal incidence, the incident wave is TM polarized, and its frequency is close to that of the symmetric quasi-TE mode or antisymmetric quasi-TM mode. As mentioned in the beginning of this subsection, a mode can be excited by normally incident light only if it possesses the symmetric in-plane components of the electromagnetic field of an incident wave. For this reason, the symmetric quasi-TE and the antisymmetric quasi-TM modes cannot be excited by a normally incident TM wave, and therefore, for them, $|\psi_{\text{res}}^{(\text{in})}\rangle = 0$ and $a_r = 0$. Thus, in this case, no resonances and no magnetically induced resonant changes are present in the optical far-field spectra.

Case III. Normal incidence, the incident wave is TM polarized, and its frequency is close to that of the symmetric quasi-TM mode. In this case, similar to Eq. (39), we obtain

$$\begin{aligned}|\psi^{(\text{in})}\rangle = \begin{pmatrix}0\\1_s\end{pmatrix} &= [O(1)+O(g^2)]\begin{Bmatrix}O(g)_a\\[1+O(g^2)]_s\end{Bmatrix}_{\text{res}}\\ &+[O(1)+O(g^2)]\begin{Bmatrix}O(g)_a\\[1+O(g^2)]_s\end{Bmatrix}_{nr}\\ &+O(g)\begin{Bmatrix}[1+O(g^2)]_a\\O(g)_s\end{Bmatrix}_{nr},\end{aligned} \tag{42}$$

where the quantities $O(g)$ are related to $F(\kappa,z)$, and therefore

$$\begin{aligned}A_{TM}(\omega) &= \frac{[O(1)+O(g^2)]^2}{\omega-\omega_0+O(g^2)}\\ &\quad+[O(1)+O(g^2)]^2+O(g)\cdot O(g)\\ &= \frac{O(1)}{\omega-\omega_0}+\frac{O(g^2)}{\omega-\omega_0}+\frac{O(g^2)}{(\omega-\omega_0)^2}\\ &\quad+O(1)+O(g^2).\end{aligned} \tag{43}$$

Again, $A_{TE}(\omega)=0$, for the same reason as in Case I. Equation (43) shows that, here, there are no magnetization-induced resonances, but the amplitude of the resonance is still influenced by the magnetization, and its dependence on g is also quadratic. So the even-in-magnetization intensity effect is present, as in the Case I.

Case IV. Normal incidence, the incident wave is TM polarized, and its frequency is close to the frequencies of both antisymmetric quasi-TE mode and the symmetric quasi-TM mode. Such a situation occurs if the resonances of the antisymmetric quasi-TE mode and the symmetric quasi-TM mode almost coincide. Following an analysis path similar to that used in deriving Eqs. (36)–(43) for the TM-polarized normally incident wave, we obtain

$$\begin{aligned}|\psi^{(\text{in})}\rangle = \begin{pmatrix}0\\1_s\end{pmatrix} &= [O(1)+O(g^2)]\begin{Bmatrix}O(g)_a\\[1+O(g^2)]_s\end{Bmatrix}_{\text{res}}\\ &+O(g)\begin{Bmatrix}[1+O(g^2)]_a\\O(g)_s\end{Bmatrix}_{\text{res}}\\ &+[O(1)+O(g^2)]\begin{Bmatrix}O(g)_a\\[1+O(g^2)]_s\end{Bmatrix}_{nr}\\ &+O(g)\begin{Bmatrix}[1+O(g^2)]_a\\O(g)_s\end{Bmatrix}_{nr},\end{aligned} \tag{44}$$

$$\begin{aligned}A_{TM}(\omega) &= \frac{O(1)}{\omega-\omega_0^{(TM)}}+\frac{O(g^2)}{\omega-\omega_0^{(TM)}}+\frac{O(g^2)}{\left(\omega-\omega_0^{(TM)}\right)^2}\\ &\quad+\frac{O(g^2)}{\omega-\omega_0^{(TE)}}+\frac{O(g^2)}{\left(\omega-\omega_0^{(TE)}\right)^2}+O(1)+O(g^2).\end{aligned} \tag{45}$$

Here, $\omega_0^{(TM)}$ and $\omega_0^{(TE)}$ are the complex frequencies of the antisymmetric quasi-TE and the symmetric quasi-TM modes, respectively. Even if the resonances are coincident, the imaginary parts of their eigenfrequencies are different since the quality factors of the two modes are not the same. Therefore, Eq. (45) demonstrates simultaneous independent presence of the two magneto-optical resonant contributions. Moreover, if the quasi-TE and quasi-TM modes additionally have the same diffraction order m_0 [see Eq. (20)], the functions $F(\kappa,z)$ and $G(\kappa,z)$ and the corresponding coefficients $O(g)$ in Eq. (44) grow higher, and hence, enhancement of the intensity effect can be expected. This is also supported by the qualitative reasoning that, at the coincidence of the quasi-TE and quasi-TM resonances, the coupling between the TE and TM components of the electromagnetic field becomes more efficient.

Case V. Normal incidence, the incident wave is TE polarized. In this case, the magneto-optical properties are generally the same, i.e. similar effects are produced by the symmetric quasi-TE and the antisymmetric quasi-TM modes. However, the magnitudes of the effects are different because of the difference in all of the coefficients in Eqs. (37)–(45). This difference mainly comes from the difference between $F(\kappa,z)$ and $G(\kappa,z)$ in Eqs. (15) and (16).

Case VI. Oblique incidence. The even-in-magnetization intensity effect also takes place at oblique incidence. An analysis similar to that of Eqs. (36)–(45) can be easily performed for oblique incidence. It should be taken into account that there are no longer any spatial parity properties for both the eigenmodes and for the incident wave, so the effect occurs at any quasi-TE and quasi-TM modes. Note that $A_{TE}(\omega)$ is no longer zero for TM-polarized incident light, but is now linear in g. So its contribution to the far-field intensity [Eq. (33)] is quadratic in g, and the effect keeps its even-in-magnetization parity.

However, at oblique incidence, another effect may additionally originate that is odd-in-magnetization. For its consideration, we neglect all quantities quadratic in g. Assume that the incident light has arbitrary linear polarization, defined by

the angle ψ. If its frequency is close to that of the quasi-TE mode, then Eq. (34) takes the following form:

$$\begin{aligned}|\psi^{(\mathrm{in})}\rangle &= \begin{pmatrix}\sin\psi\\ \cos\psi\end{pmatrix}\\ &= [O(1)\sin\psi + O(g)\cos\psi]\begin{bmatrix}1\\ O(g)\end{bmatrix}_{\mathrm{res}}\\ &\quad + [O(1)\sin\psi + O(g)\cos\psi]\begin{bmatrix}1\\ O(g)\end{bmatrix}_{nr}\\ &\quad + [O(1)\cos\psi + O(g)\sin\psi]\begin{bmatrix}O(g)\\ 1\end{bmatrix}_{nr}. \end{aligned} \tag{46}$$

The far-field amplitudes have the following form:

$$\begin{aligned}A_{TM}(\omega) &= \frac{O(g)\sin\psi}{\omega-\omega_0} + O(g)\sin\psi + O(1)\cos\psi\\ &= O(1)\cos\psi + O(g)\sin\psi\left[\frac{O(1)}{\omega-\omega_0} + O(1)\right],\\ A_{TE}(\omega) &= \frac{O(1)\sin\psi + O(g)\cos\psi}{\omega-\omega_0}\\ &\quad + O(1)\sin\psi + O(g)\cos\psi\\ &= O(1)\sin\psi\left[\frac{O(1)}{\omega-\omega_0} + O(1)\right]\\ &\quad + O(g)\cos\psi\left[\frac{O(1)}{\omega-\omega_0} + O(1)\right]. \end{aligned} \tag{47}$$

Similarly, if the frequency corresponds to the excitation of the quasi-TM mode then

$$\begin{aligned}|\psi^{(\mathrm{in})}\rangle &= \begin{pmatrix}\sin\psi\\ \cos\psi\end{pmatrix} = [O(1)\cos\psi + O(g)\sin\psi]\begin{bmatrix}O(g)\\ 1\end{bmatrix}_{\mathrm{res}}\\ &\quad + [O(1)\cos\psi + O(g)\sin\psi]\begin{bmatrix}O(g)\\ 1\end{bmatrix}_{nr}\\ &\quad + [O(1)\sin\psi + O(g)\cos\psi]\begin{bmatrix}1\\ O(g)\end{bmatrix}_{nr}, \end{aligned} \tag{48}$$

$$\begin{aligned}A_{TM}(\omega) &= O(1)\sin\psi + O(g)\cos\psi\left[\frac{O(1)}{\omega-\omega_0} + O(1)\right],\\ A_{TE}(\omega) &= O(1)\cos\psi\left[\frac{O(1)}{\omega-\omega_0} + O(1)\right]\\ &\quad + O(g)\sin\psi\left[\frac{O(1)}{\omega-\omega_0} + O(1)\right]. \end{aligned} \tag{49}$$

According to Eqs. (47) and (49), for the excitation of both types of modes, the far-field intensity is given by

$$\begin{aligned}I(\omega) &\propto |A_{TM}(\omega)|^2 + |A_{TE}(\omega)|^2\\ &\cong A_0^2(\omega) + O(g)\sin 2\psi\\ &\quad \times \mathrm{Re}\left[\frac{O(1)}{\omega-\omega_0} + \frac{O(1)}{(\omega-\omega_0)^2} + O(1)\right], \end{aligned} \tag{50}$$

where $A_0^2(\omega)$ is the intensity for the nonmagnetized structure. So, compared to Eq. (6), we find that there is an odd-in-magnetization intensity effect, described by

$$\begin{aligned}\delta_{\mathrm{odd}}(\omega) &= \frac{I(g,\omega) - I(-g,\omega)}{I(0,\omega)}\\ &\propto O(g)\sin 2\psi\,\mathrm{Re}\left[\frac{O(1)}{\omega-\omega_0} + \frac{O(1)}{(\omega-\omega_0)^2} + O(1)\right]. \end{aligned} \tag{51}$$

Equation (51) demonstrates that this resonance-triggered effect emerges when both quasi-TE and quasi-TM modes are excited and only for intermediate incident polarization, while vanishing at $\sin 2\psi = 0$ (the latter is fulfilled for s and p polarizations).

The vanishing of this odd effect for s and p polarizations as well as for normal incidence can easily be understood through symmetry reasoning. Indeed, under the operation $y \to -y$, the structure transforms into itself with reversed magnetization ($M \to -M$), while the incident wave vector is not changed, and the incident polarization angle changes its sign ($\psi \to -\psi$). Meanwhile, the reflection and the transmission coefficients are invariant with respect to this transformation (for details, see Appendix C), therefore

$$I(g,\psi) = I(-g,-\psi). \tag{52}$$

Comparing Eq. (52) with Eq. (6), one concludes that, for the odd effect, $\delta_{\mathrm{odd}} = 0$ at $\psi = 0$ and $\psi = \pi/2$ (since the cases of $\psi = \pi/2$ and $\psi = -\pi/2$ are equivalent).

For normal incidence and arbitrary polarization, the inversion of magnetization is equivalent to the rotation of the structure by 180° around the z axis, so $I(g,\psi) = I(-g,\psi)$ and again $\delta_{\mathrm{odd}} = 0$.

It should be noted that, though the magnetization configuration is similar to the case of the orientational effect of the conventional magneto-optics of smooth ferromagnets, the effect considered here has to be regarded as novel. Indeed, as it will be shown later, this effect has different behavior with respect to the incident light polarization. For example, it does not vanish for normally incident light polarized along the medium magnetization, while the orientational effect does. In addition to that, it is exclusively caused by the excitation of eigenmodes of the nanostructured medium so that it may be termed longitudinal magnetophotonic intensity effect (LMPIE).

III. METHODS

A. Rigorous coupled-wave analysis modeling and S-matrix

The design of the MPC and the modeling of its optical properties were performed using the rigorous coupled-wave analysis (RCWA) technique [52] extended to the case of gyrotropic materials [53]. The eigenfrequencies of the guided modes of the structure were determined by the scattering-matrix (S-matrix) method [50]. For the modeling of the experimentally studied MPC with ferrimagnetic films of $Bi_2Dy_1Fe_4Ga_1O_{12}$ and $Bi_{2.97}Er_{0.03}Fe_4Al_{0.5}Ga_{0.5}O_{12}$, the permittivity ε and the gyration g were taken from experiment and from Refs. [55] and [56] (e.g. for $Bi_2Dy_1Fe_4Ga_1O_{12}$ at $\lambda = 700$ nm, $\varepsilon_0 = 5.34 + 0.014i$, $g = (2.3 - 0.2i)\times 10^{-3}$, $b = 3\times 10^{-5}$, and for $Bi_{2.97}Er_{0.03}Fe_4Al_{0.5}Ga_{0.5}O_{12}$ at 840 nm,

$\varepsilon_0 = 6.440 + 0.012i$, $g = (15 - 0.1i) \times 10^{-3}$, and $b = 4 \times 10^{-5}$). On the other hand, for the modeling of the MPC with a ferromagnetic film of $Bi_3Fe_5O_{12}$, the optical parameters were taken from Ref. [57] (e.g. at $\lambda = 840$ nm, $\varepsilon_0 = 12.646 + 0.027i$, $g = (46 - 9i) \times 10^{-3}$). The dispersion of all quantities was taken into account. For the permittivity of gold, we used the experimental data from Ref. [58].

B. Experimental

In order to investigate the LMPIE experimentally, we fabricated an MPC heterostructure (MPC-A) with a dielectric layer composed of bismuth-substituted rare-earth iron garnet consisting of a $Bi_2Dy_1Fe_4Ga_1O_{12}$ film of thickness $h_m = 875$ nm and a gold grating (period is $d = 309$ nm, grating thickness is $h_{gr} = 50$ nm, slit width is $r = 77$ nm).

To enhance the LMPIE, another MPC sample (MPC-B) was fabricated. It contained 1270-nm-thick iron garnet film of composition $Bi_{2.97}Er_{0.03}Fe_4Al_{0.5}Ga_{0.5}O_{12}$ and a gold grating with the following parameters: $d = 661$ nm, $h_{gr} = 67$ nm, and $r = 145$ nm.

In both cases, the geometrical parameters of the MPCs were chosen to have degeneracy of the first order TM and TE modes at the Γ point ($\kappa = 0$) of the Brillouin zone (see Fig. 3 and corresponding discussion). As a consequence, both modes can be excited by normally incident light of the same frequency. The degeneracy between the TE- and the TM modes increases the coupling efficiency of the incident radiation to the quasi-TM and quasi-TE modes and leads to enhanced LMPIE (see Case IV).

The magnetic layers were deposited on a gadolinium gallium garnet (GGG) substrate by RF-magnetron sputtering followed by a high-temperature oven annealing procedure. The films showed a uniaxial magnetic anisotropy. The gold gratings were fabricated by thermal deposition of a gold layer onto the iron garnet film and subsequent electron beam lithography combined with reactive ion etching by an Ar-ion plasma.

All magneto-optical measurements were performed at room temperature. A halogen lamp was used as a white light source. The collimated light was focused onto the sample to a spot with about 300 μm diameter and an aperture angle below 1°. The sample was mounted on a rotation stage to vary the angle of incidence θ in the range from 0° to 3°. The zero-order transmission and reflection signals were dispersed with a monochromator (linear dispersion 6.28 nm/mm) and detected by a charge-coupled device detector. A magnetic field of up to 300 mT was applied in the MPC film plane and perpendicular to the grating slits. The angle ψ between the light polarization plane and normal to the slits was adjusted with a Glan-Thompson prism.

IV. RESULTS AND DISCUSSION

A. The LMPIE odd and even in magnetization

Since the magneto-optical effect considered here is strongly related to the eigenmodes excitation and mutual conversion, we begin our analysis from the consideration of the dispersion diagram for the MPC modes. Since, with regard to dispersion, the nonmagnetized and longitudinally magnetized cases are almost the same, we present here the dispersion for the TM and TE modes of the experimentally studied MPC-A in the nonmagnetized state [Fig. 3(a)], which was calculated using the S-matrix method.

The waveguide modes of the structure can be classified by their orders, i.e. by the number of peaks of H_y (for the TM modes) and E_y (for the TE modes) along the z axis. Accordingly, modes denoted by (1) are first order, by (2) are

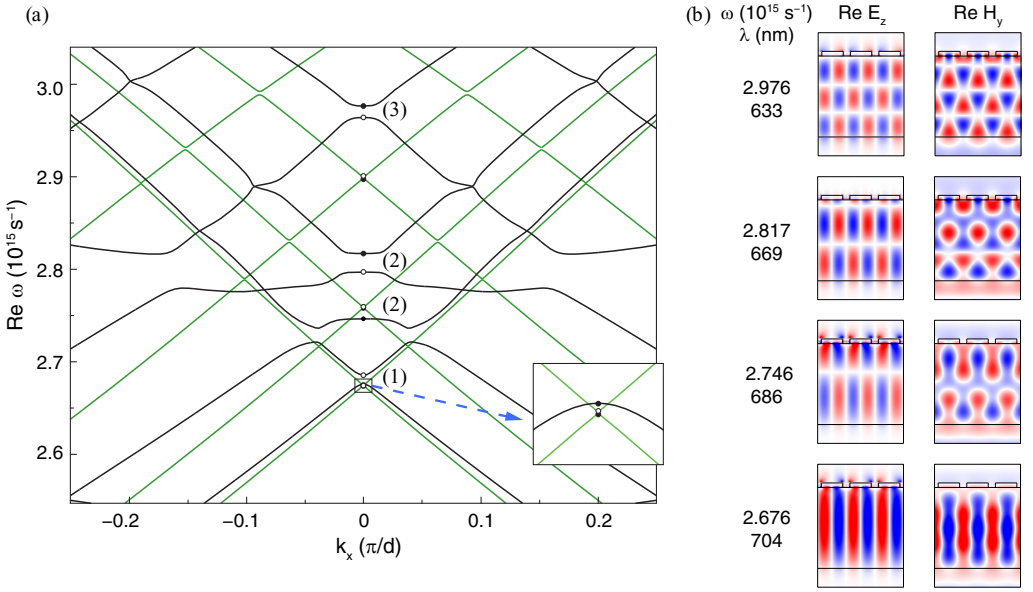

FIG. 3. (Color online) Calculated modes of the experimentally studied MPC-A in the nonmagnetized state. (a) Dispersion of the TM (black curves) and TE modes (green curves) calculated by the S-matrix method. Inset shows a region at around the Γ point where degeneration of the TM and TE modes takes place. Filled and open circles indicate symmetric and antisymmetric modes, respectively. Numbers (1)–(3) refer to the mode orders (see the text). (b) Color plots showing electromagnetic field distributions of different symmetric TM modes at the Γ point. The real parts of E_z and H_y field components are shown. All values are normalized to the unity.

second order, and so on, as seen from H_y field distributions for the TM modes shown in Fig. 3(b). All resonances are excited by the first diffraction order in the magnetic layer. The symmetry of the modes at the Γ point is indicated by filled circles for even parity and by open circles for odd parity in Fig. 3(a).

The only electric field component (E_y) of the TE modes is tangential to the magnetic layer interfaces. On the other hand, the TM modes have an electric field component (E_z) normal to the magnetic film interfaces. Consequently, in accordance to the boundary conditions, the TE modes are less sensitive to the perforation of the gold layer adjacent to the magnetic layer. This results in TE modes with narrower resonances and larger quality factors than those of the TM modes. The dispersion curves of the TE modes are also much closer to the dispersion for the waveguide with smooth surrounding media. On the contrary, the dispersion curves of the TM modes deviate significantly from the case of the smooth structure. In particular, the perforation of gold gives rise to several rather broad stop bands. The TM modes have plasmonic character, which manifests in the field localization near the interface with the gold grating [Fig. 3(b)].

Apart from waveguide TM resonances, there can be localized TM modes near gold stripes of the grating. In the experimentally studied MPC, the hybridization of the waveguide and localized modes takes place in the spectral region from $2.73 \times 10^{15}\mathrm{s}^{-1}$ to $2.82 \times 10^{15}\mathrm{s}^{-1}$ [Fig. 3(a)]. As a result, at the Γ point, two modes appear, namely the one at $2.746 \times 10^{15}\mathrm{s}^{-1}$, having mostly localized character, and the other one at $2.817 \times 10^{15}\mathrm{s}^{-1}$, having mostly waveguide character. This is confirmed by the corresponding distributions of H_y and E_z [Fig. 3(b)].

One distinct feature of the MPC is that its first-order symmetric TM mode and its symmetric and antisymmetric TE modes have almost equal eigenfrequencies at the Γ point [see inset in Fig. 3]. This corresponds to the excitation wavelength $\lambda = 705$ nm.

The transmission spectrum for the TM-polarized illumination ($\psi = 0^{\mathrm{o}}$) in the considered wavelength range has three Fano resonances related to the excitation of the symmetric TM modes [upper curve in Fig. 4(a)]. Interestingly, the Fano spectral line around 675 nm is caused by the interference of two second-order resonances related to excitation of hybridized waveguide and localized modes.

Symmetric TE modes give rise to Fano resonances in the transmission spectrum for the TE-polarized illumination ($\psi = 90^{\mathrm{o}}$), though not so pronounced as in the case of TM-incident polarization [upper curve in Fig. 4(b)]. For light incidence close to normal, the antisymmetric modes are not excited due to symmetry, and consequently, there is no sign of them in the observed transmission spectra.

An incident light with intermediate polarization, given by $\psi = 36^{\circ}$, excites both TE and TM modes, thus leading to a transmission spectrum with resonances related to both modes [upper curve in Fig. 4(c)]. This is mostly evident for the resonances related to the third-order TM and TE modes since they are about 10 nm apart. The transmission spectrum at $\psi = 36^{\circ}$ has two features at 639 nm (TM resonance) and 649 nm (TE resonance).

If an external magnetic field of sufficient strength is applied in-plane and perpendicular to the slits in the gold grating, then the magnetic layer of the MPC becomes uniformly magnetized, thus modifying the transmission spectra and triggering the LMPIE around wavelengths corresponding to the excitation of the quasi-TE modes [lower curves in Fig. 4].

Both odd and even LMPIE have the largest values at the degenerate resonance (at 705 nm) where the quasi-TM and quasi-TE modes of the MPC are excited simultaneously. At this wavelength, the value of the even LMPIE (δ_{even}) reaches 0.6%. This validates our theoretical predictions made in Sec. II.D [see Eq. (45) and the corresponding discussion].

For TM- or TE-polarized illumination, only the even LMPIE is present [thick red curves in Figs. 4(a) and 4(b)]. The odd effect appears only for intermediate polarizations [e.g. for

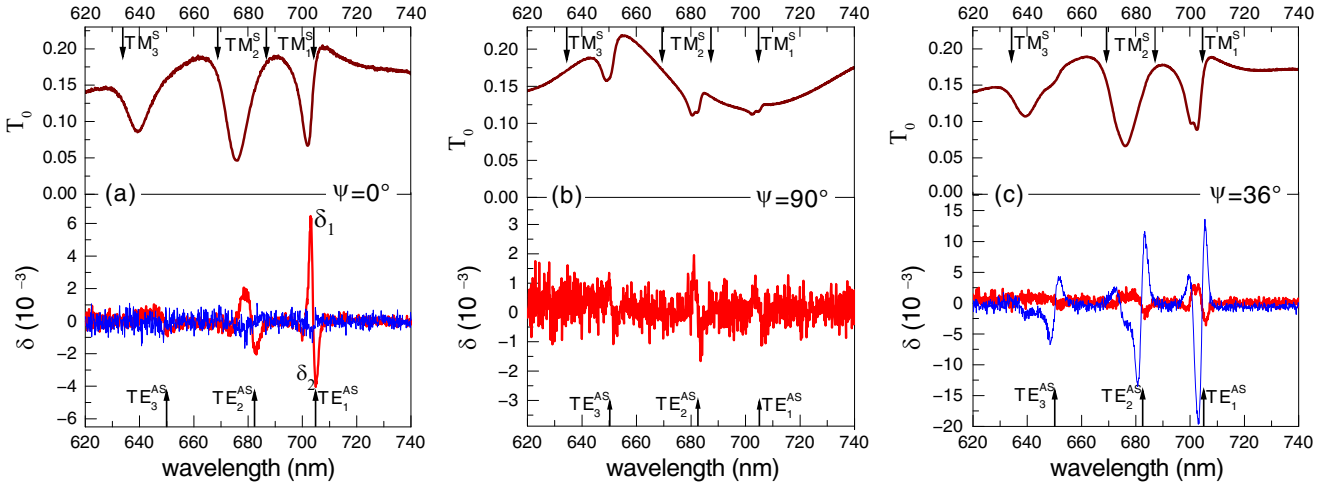

FIG. 4. (Color online) Measured spectra of transmission through the demagnetized MPC-A T_0 (upper brown curves) as well as odd (thin blue curves) and even (thick red curves) LMPIE at three different polarization angles: (a) $\psi = 0°$, (b) $\psi = 90°$, and (c) $\psi = 36°$. Incidence angle was about 0.3°. The LMPIE was measured at an external magnetic field of 160 mT. Arrows indicate the spectral positions of the TE and TM resonances taken from their calculated dispersion in Fig. 3. In the notation of TM and TE modes, the upper index shows the mode symmetry, while the bottom one indicates the mode order.

$\psi = 36^\circ$, Fig. 4(c)] as soon as the space symmetry of the illumination is broken, i.e. when light hits the sample at slightly oblique angle. The odd effect is already rather large for small incidence angle $\theta = 0.3^\circ$ and only marginally increases for larger incidence angles. In this sense, the odd LMPIE is quite different from the conventional odd magneto-optical effects, which pronouncedly increase for oblique incidence and reach maximal values around $\theta = 50^\circ \div 60^\circ$ [3].

B. Near-field aspect of the LMPIE

As seen from the discussion above and the experimental data, the LMPIE is induced by the modification of the optical near-field by the longitudinal magnetization. Since both odd and even LMPIE are caused by the same modes, we focus our discussion in the following subsection on the even LMPIE only.

The electromagnetic field distribution for the TM-polarized illumination at the combined TE- and TM-mode resonances (at $\lambda = 705$ nm) for the nonmagnetized and longitudinally magnetized MPCs reveals the appearance of the quasi-TE mode in the latter case [Figs. 5(a) and 5(b)]. This is demonstrated through the emergence of the E_y field component (directed along the slits in the gold grating), which is one of the main components of the quasi-TE mode [Fig. 5(b)]. The spatial distribution of E_y is the same as the distribution of E_y in the quasi-TE mode [Figs. 5(b) and 5(c)]. After magnetizing the MPC, the field distribution of the H_y component remains almost unchanged [compare Figs. 5(e) and 5(f)]. This means that the LMPIE related to the quasi-TM mode resonance is very weak.

The excited quasi-TE mode has an antisymmetric component E_y [Fig. 5(c)] and a symmetric magnetically induced H_y component [Fig. 5(d)]. Therefore, the LMPIE is related to the antisymmetric quasi-TE-mode. This is due to the fact that, at normal incidence, the TM-polarized light can excite only symmetric in-plane electromagnetic field components which are contained in the antisymmetric quasi-TE mode. Thus, the unique feature of the considered MPC is that the longitudinally applied magnetic field allows the excitation of the TE field components by the TM-polarized light. Moreover, the quasi-TE mode with antisymmetric main in-plane components is excited by the symmetric light which is impossible for the nonmagnetized case.

For the experimental sample, the symmetric and antisymmetric TE-mode resonances are positioned very close to each other. To investigate the interconnection between modes symmetry and LMPIE, let us consider that the MPC is designed to have symmetric and antisymmetric TE and TM resonances sufficiently separated from one another (Fig. 6). Based on the above reasoning, it is obvious that the largest LMPIE appears near the frequencies of the antisymmetric TE modes [Fig. 6(a)].

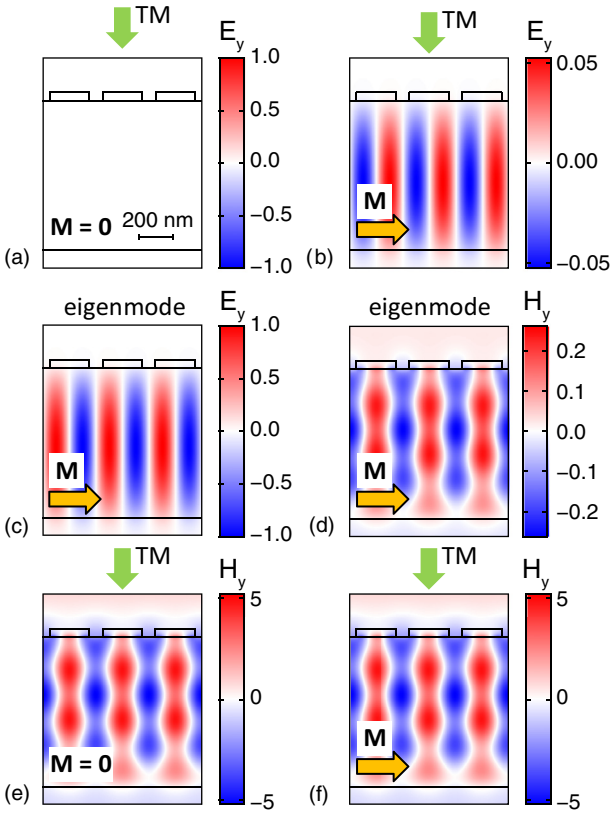

FIG. 5. (Color online) Color plots of the electromagnetic field distribution in the near field of the MPC-A. E_y field inside the (a) nonmagnetized and (b) magnetized structure in the case of TM-polarized normally incident light at $\lambda = 705$ nm. The field is normalized by H_y of the incident light. (c) E_y and (d) H_y of the quasi-TE mode in the magnetized structure. H_y field inside the (e) nonmagnetized and (f) magnetized structure in the case of TM-polarized normally incident light at $\lambda = 705$ nm.

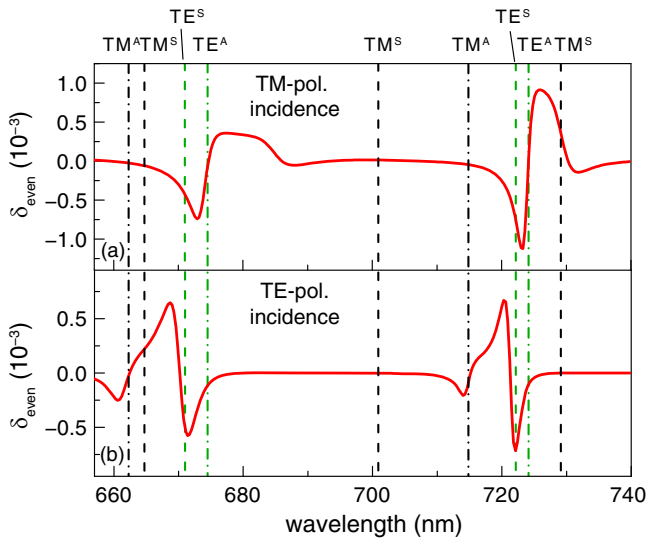

FIG. 6. (Color online) The even LMPIE calculated for an MPC with the magnetic film of composition $Bi_2Dy_1Fe_4Ga_1O_{12}$ and a gold grating with the following parameters: $d = 360$ nm, grating thickness is $h_{gr} = 63$ nm, slit width is $r = 270$ nm. (a) The incident wave is TM polarized, (b) the incident wave is TE polarized. Vertical lines indicate the spectral positions of the TM modes (black lines) and TE modes (green lines), which are symmetric (dashed lines) and antisymmetric (dash-dotted lines). The light is normally incident. The optical and magneto-optical parameters of the MPC are the same as for the experimental sample.

TABLE II. Relation between the value of the LMPIE and type and symmetry of the modes.

Type of a mode	TM-polarized light	TE-polarized light
Symmetric quasi-TM	"weak"	–
Antisymmetric quasi-TM	–	"weak"
Symmetric quasi-TE	–	"strong"
Antisymmetric quasi-TE	"strong"	–

Since the magnetic field also modifies the TM modes, one should expect some LMPIE around the symmetric quasi-TM resonances. Note that the LMPIE is also present there, but its value is significantly smaller (by about two orders of magnitude) relative to the effect at the TE-mode resonance. Antisymmetric quasi-TM modes and symmetric quasi-TE modes provide no LMPIE since, for symmetry reasons, they cannot be excited in this configuration.

Now let us discuss the case of the TE-polarized light [Fig. 6(b)]. Expanding the above reasoning to this case implies that the LMPIE should appear now around the resonances of the antisymmetric quasi-TM mode, since the external magnetic field induces it to contain symmetrical TE components. For the MPC considered here, the LMPIE is observed around 662 and 716 nm. However, the largest effect corresponds again to the quasi-TE modes (at 670 and 722 nm) as for the case of TM-polarized light, but this time these quasi-TE modes are symmetric.

As discussed in Sec. II, the LMPIE appears at a mode excitation because of the magnetization-induced electromagnetic field components of orthogonal polarization. Since the quasi-TE modes usually have quality factors higher than the ones of the quasi-TM modes, the TM $\rightarrow$ TE conversion is more efficient than the TE $\rightarrow$ TM conversion. Therefore, the LMPIE is highest at the TE-mode resonances, and this explains the LMPIE behavior shown in Fig. 6. This reasoning is also supported by direct calculation of the F and G that are responsible for the TE-TM conversion at the quasi-TM and quasi-TE modes, respectively [see Eqs. (15) and (16)]. For example, for the TM resonance at 716 nm, $|F| \approx 0.04$, and for the TE resonance at 720 nm, $|G| \approx 0.001$ (at the point $z = 0$).

The main results of the analysis of the LMPIE relation to the mode symmetries are summarized in Table II.

C. Properties of the odd and even LMPIE

Dependence of the peak values of δ_{even} and δ_{odd} at $\lambda = 703$ nm and $\lambda = 705$ nm on ψ are shown in Fig. 7. It is seen that the odd LMPIE exhibits maximum magnitude at around $\psi = 35^\circ$, while the even LMPIE is largest at $\psi = 0^\circ$.

The above results can be explained as follows: Eq. (52) demands that the ψ dependence of δ_{odd} must be odd, and δ_{odd} must vanish at $\psi = 0^\circ$ and $\psi = 90^\circ$. The present behavior of δ_{odd} is in excellent agreement with that. Furthermore, the ψ dependence of δ_{odd} has the form of $\sin 2\psi$ as predicted by Eq. (51). However, all of the coefficients $O(g)$ and $O(1)$ in Eq. (51) are also ψ dependent, so δ_{odd} is not directly proportional to $\sin 2\psi$.

The higher efficiency of the TM $\rightarrow$ TE conversion than the reverse conversion explains the larger value of the even LMPIE for $\psi = 0^\circ$ than for $\psi = 90^\circ$.

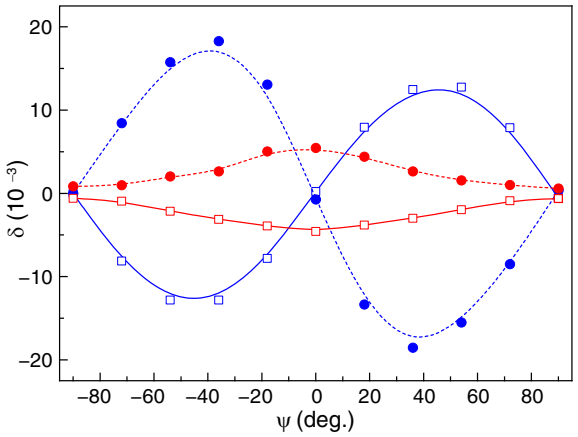

FIG. 7. (Color online) Experimentally measured for the MPC-A odd (blue symbols) and even (red symbols) LMPIE versus the polarization angle ψ at $\lambda = 703$ nm (filled circles) and $\lambda = 705$ nm (open squares). Incidence angle is 0.3°. External magnetic field is 160 mT. Solid and dashed lines are meant as guides to the eyes.

The even LMPIE is largest for normal incidence when the TM- and TE-mode resonances are closest; the spectral distance between them at the Γ point of the Brillouin zone is 0.6 nm only around $\lambda = 705$ nm [Fig. 8(a)]. The spectral proximity of the quasi-TE and quasi-TM modes provides efficient TM $\rightarrow$ TE conversion. At normal incidence, the resonance value of δ_{even} is 8×10^{-3} at saturation [Fig. 8(b)]. For oblique incidence, the resonances get separated, and the LMPIE effect reduces. At $\theta = 1^\circ$, the spectral separation between the TM and TE resonances is 2.0 nm, and δ_{even} does not exceed 3×10^{-3} [Fig. 8(a)]. Interestingly, another increase of the LMPIE (δ_{even} is 4×10^{-3}) happens at $\theta = 3^\circ$ when the first-order TE-mode resonance coincides with the resonance of the second-order TM mode [Figs. 8(a) and 8(b)].

It should be noted that the intersection of the dispersion of the TM and TE modes at $\lambda = 682$ nm at normal incidence gives a several-times-smaller LMPIE than at $\lambda = 705$ nm. This is due to the larger wavelength separation between the two resonances, namely 3.0 nm.

The magnetization of the dielectric layer of the MPC is proportional to the external magnetic field up to the fields of about $B = 120$ mT. For larger B fields, the magnetization starts to saturate, and the magnetic substrate becomes fully saturated at $B \sim 240$ mT. For $B < 120$ mT, the even LMPIE is quadratic in B, proving that it is second order in M (Fig. 9).

D. Approaches to LMPIE enhancement

Since the even LMPIE is second order in M, its value of around 10^{-2} can be already considered quite large. This becomes even more evident if compared with the orientational effect which is also quadratic in M. For a smooth iron-garnet film, the orientational effect is extremely small: $\delta \sim 10^{-5}$ (as calculated for $\theta = 0^\circ$ and $\psi = 90^\circ$). For ferromagnetic metals, it reaches maximum values of $\delta \sim 10^{-3}$ [6].

However, the even LMPIE can be enhanced dramatically when a magnetic layer with a high value of g and a low absorption coefficient α is used, thus opening the way for new practical applications, such as high-speed optical

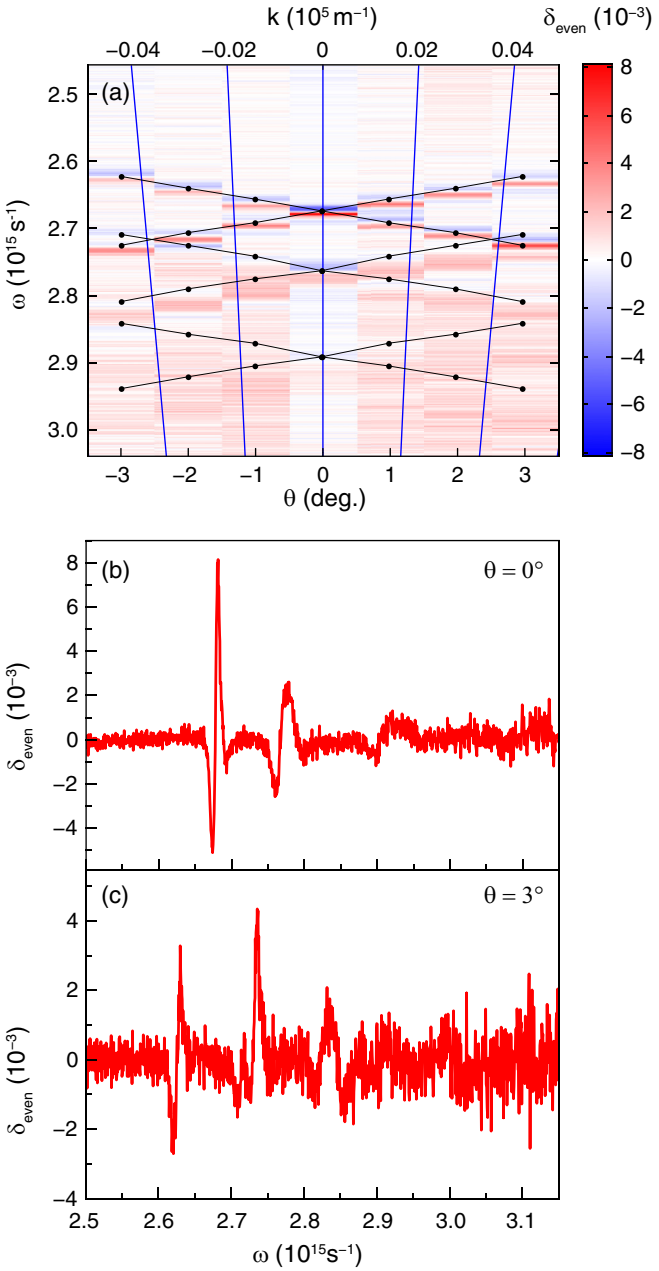

FIG. 8. (Color online) Experimentally measured angle dispersion for the even LMPIE. (a) Color plot for δ_{even} versus incidence angle and illumination light frequency. Blue lines connect points of equal k. Black lines with dots indicate calculated dispersion of the quasi-TE modes. Spectral dependence of δ_{even} for (b) normal and (c) oblique incidence ($\theta = 3^{o}$). Incident light is TM polarized. External magnetic field is 240 mT.

switches and modulators as well as magneto-optical sensors. The even LMPIE for the MPC-B, having an iron-garnet layer with almost full substitution by Bi (the composition is $Bi_{2.97}Er_{0.03}Fe_4Al_{0.5}Ga_{0.5}O_{12}$), reaches $\delta = 0.24$, which is about 30 times larger than the one for the MPC-A [46] [Fig. 10(a)]. The reason for that is 6 times larger gyration and 2 times smaller optical absorption ($g = 0.015, \alpha = 400$ cm^{-1} at 840 nm) of the magnetic layer. The odd LMPIE for the MPC-B is enhanced as well, though, in this case, the enhancement factor is not so high and is about 4 times [Fig. 10(b)].

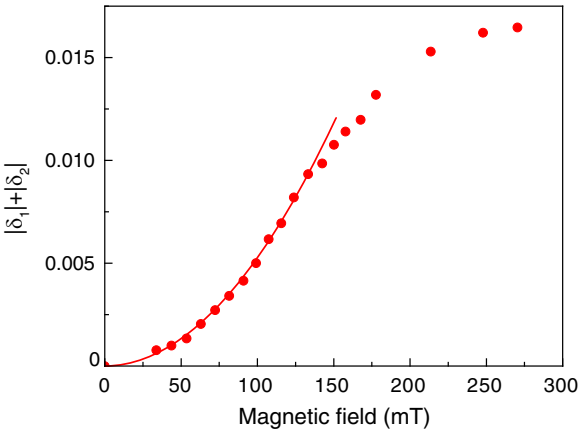

FIG. 9. (Color online) Experimentally measured magnetic field dependence of the even LMPIE in the MPC-A. The even LMPIE is represented here by $|\delta_1| + |\delta_2|$ (circular symbols), where δ_1 and δ_2 are the positive and negative peaks of the even LMPIE at $\lambda = 703$ and 705 nm, respectively [see Fig. 4(a)]. Solid line is a parabolic fit. Incident light is TM polarized and normally incident.

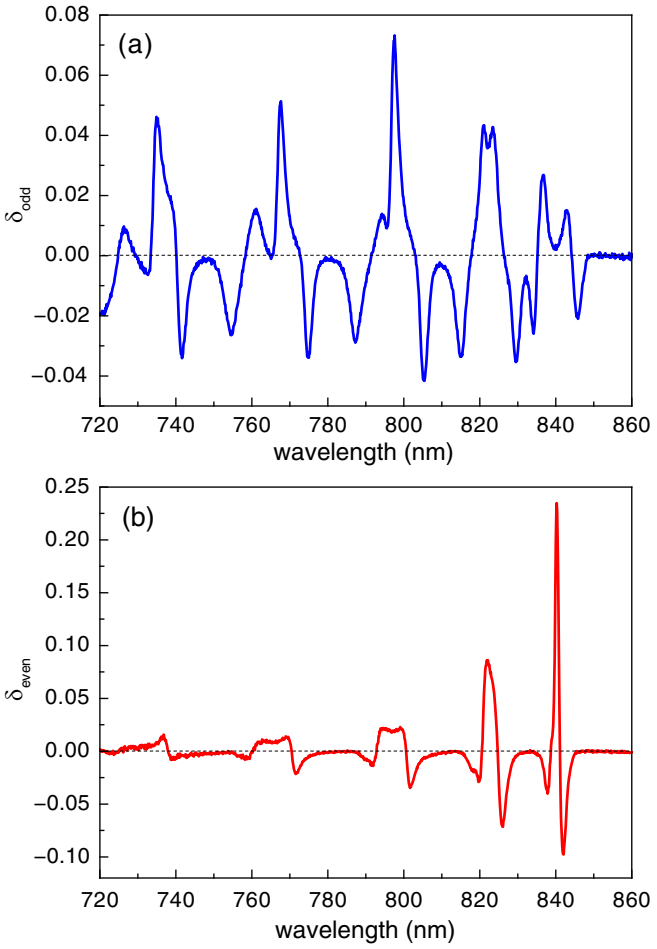

FIG. 10. (Color online) Measured spectra of (a) odd and (b) even LMPIE for the MPC-B. (a) The polarization angle is $\psi = 36°$, and the incidence angle of light incidence is $\theta = 1°$; (b) $\psi = 0°$, and light is normally incident. $B = 160$ mT.

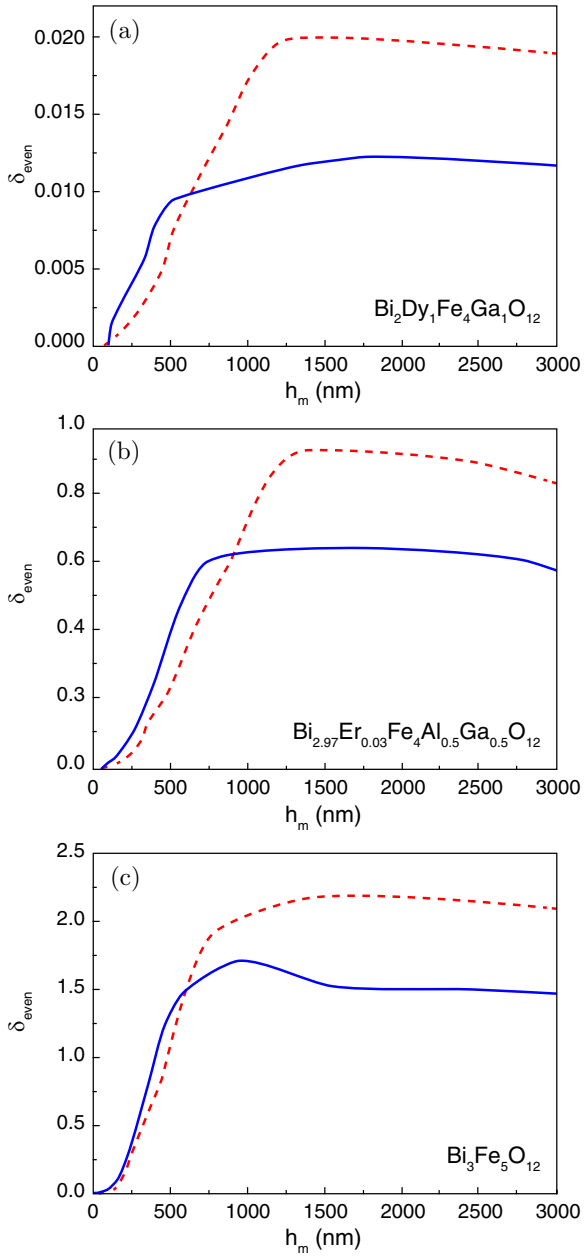

FIG. 11. (Color online) Calculated maximum achievable value of the even LMPIE in transmission (solid blue curves) and in reflection (dashed red curves) versus the thickness of the magnetic layer h_m. All other geometrical parameters of the MPC were varied to get the largest possible value of δ_{even} at the wavelengths range of 650–900 nm with the condition that $T(0) > 10\%$. MPCs with magnetic films of three different compositions are considered: (a) $Bi_2Dy_1Fe_4Ga_1O_{12}$, (b) $Bi_{2.97}Er_{0.03}Fe_4Al_{0.5}Ga_{0.5}O_{12}$, and (c) $Bi_3Fe_5O_{12}$ (see Sec. III.B). The light hits the sample under normal incidence and is TM polarized. It is assumed that an external magnetic field saturates magnetization of the magnetic film.

Furthermore, magnetic dielectrics of even better magneto-optical quality could lead to the LMPIE exceeding 100% as is predicted by calculations for the MPC with a magnetic layer of $Bi_3Fe_5O_{12}$ having record but still realistic parameters: $g = 0.049$ and $\alpha = 580$ cm^{-1} at 805 nm [57] [Fig. 11(c)].

The other possibility to increase the LMPIE effect is to use a magnetic layer of larger thickness. Indeed, the calculated dependence of the maximum possible magnitude of the even LMPIE on h_m predicts that the largest values of δ_{even} are achievable for $h_m > 1000$ nm (Fig. 11, Table III). The increase of δ_{even} with h_m can be understood by exploring the behavior of the function $G(\kappa,z)$ that defines the TM $\rightarrow$ TE conversion efficiency [according to Eqs. (15) and (16)].

Calculations reveal that the functions $F(\kappa,z)$ and $G(\kappa,z)$ monotonically increase with h_m. For example, for $h_m =$ 300 nm, $|G| = 0.03$, and for $h_m = 1000$ nm, $|G| = 0.7$ (for the single mode at the point $z = 0$). Obviously, for a thicker magnetic layer, the proposed linear in g approximation for analysis of the MPC modes is no longer applicable. So, further increasing h_m leads to more losses which diminish the figure of merit for the quasiwaveguide modes. That is why the growth of the even LMPIE stops at some h_m value and decreases slightly beyond that value. Comparing different plots of Fig. 11, one can see that the optimal value of h_m depends on the magnetic film composition, but the general trend remains valid.

The maximum achievable value of the even LMPIE in reflection is larger than in transmission (see dashed brown curves in Fig. 11 and Table III). Thus, for the MPC with a magnetic layer of $Bi_3Fe_5O_{12}$, δ_{even} surpasses 2 for $h_m \sim$ 1400 nm [Fig. 11(c), Table III], which represents great promise for future applications.

V. CONCLUSION

In this paper, we have investigated a novel effect related to the influence of the magnetic field on the optical transmission of light through an MPC consisting of a gold layer periodically perforated with a slit array and a magnetic layer magnetized perpendicularly to the slits. It has been demonstrated that this effect has near-field and far-field aspects and that the magnetization modifies the optical modes of the MPC leading to the possibility of antisymmetric quasi-TE mode excitation by TM-polarized light. It has also been shown that antisymmetric TE mode in the nonmagnetized structure cannot be excited by normal light incidence of any polarization; thus, an external magnetic field makes this "dark" mode "bright".

In addition, it has been demonstrated that the far-field aspect of the observed effect is displayed obviously through the modification of the optical transmission and reflection spectra when the magnetic layer is magnetized, thus justifying the proposed denomination of this effect as longitudinal magnetophotonic intensity effect (LMPIE).

The LMPIE has been shown to have both odd and even contributions in magnetization. The even LMPIE is present for any incident light configuration, while the odd one is observed only for oblique incidence of the light having both TM- and TE-polarization components, i.e. for $0^\circ < \psi < 90^\circ$. Results have also shown that the LMPIE displays maximum values in the case when resonances of the TM and TE modes coincide and the most efficient conversion of the incident TM-polarized illumination into the quasi-TE mode takes place.

The even LMPIE has been shown to be quadratic in the medium gyration g, and due to that, it can be significantly increased by using materials with larger gyration g and lower absorption coefficient α. Moreover, since the maximum

TABLE III. Geometrical parameters of the MPCs (magnetic film thickness h_m, gold grating period d, grating thickness h_{gr}, slit width r) for maximum achievable magnitude of the even LMPIE in transmission and in reflection for the MPCs with magnetic films of three different compositions. The resonances of the even LMPIE were searched at wavelength range of 650–900 nm with the condition that $T(0) > 10\%$. The light hits the sample under normal incidence and is TM polarized. All geometrical parameters and wavelength are measured in nanometers.

		h_m	d	h_{gr}	r	λ	δ_{even}
$Bi_2Dy_1Fe_4Ga_1O_{12}$	Transmission	1763	357	66	232	801	0.012
	Reflection	1567	360	113	75	811	0.020
$Bi_{2.97}Er_{0.03}Fe_4Al_{0.5}Ga_{0.5}O_{12}$	Transmission	1761	356	84	52	900	0.65
	Reflection	1398	356	151	182	898	0.94
$Bi_3Fe_5O_{12}$	Transmission	947	239	74	60	821	1.71
	Reflection	1394	242	83	79	821	2.17

achievable even LMPIE is sensitive to the magnetic layer thickness, the LMPIE can be additionally increased by choosing an optimum value for the thickness.

The theoretically investigated and experimentally demonstrated novel magneto-optical effect can be used for modern telecommunication devices since it enables light intensity modulation at gigahertz frequencies and allows switching between the different modes of the structure. The latter is of prime importance for the realization of high-performance integrated optical devices and structures and their deployment in emerging optical switching applications.

ACKNOWLEDGMENTS

The work was supported by the Deutsche Forschungsgemeinschaft (Project No. AK40/7-1), the Russian Foundation for Basic Research (Project Nos. 13-02-01122, 13-02-91334, 13-02-92710, and 13-02-90438). V.I.B. acknowledges support from the Alexander von Humboldt Foundation. A.N.K. acknowledges support from the Russian Presidential Fellowship (No. SP-124.2012.5).

APPENDIX A: THE WAVEGUIDE MODES IN THE PRESENCE OF MAGNETIZATION

The waveguide modes in longitudinally magnetized planar waveguide acquire field components as shown by Eqs. (15) and (16). The explicit formulas for $F(\kappa,z)$ and $G(\kappa,z)$ have rather complicated form. For example, for the coordinate $z = z_1$ corresponding to the metal/magnetic interface, they are the following (see the main text for the notations):

$$F(\kappa,z_1) = i\frac{\kappa\omega\left[\left(\varepsilon_0\gamma_1+\varepsilon_1\gamma_3\right)h_m\sin\left(\gamma_2 h_m\right)-\frac{1}{\gamma_2}\left(\varepsilon_0\gamma_1\gamma_3-\varepsilon_1\gamma_2^2\right)h_m\cos\left(\gamma_2 h\right)+\frac{1}{\gamma_2^2}\left(\varepsilon_0\gamma_1\gamma_3+\varepsilon_1\gamma_2^2\right)\sin\left(\gamma_2 h_m\right)\right]}{2c\varepsilon_1\varepsilon_0\gamma_2\gamma_3\left[\left(1+\frac{\gamma_1}{\gamma_3}\right)\cos\left(\gamma_2 h_m\right)+\left(\frac{\gamma_1}{\gamma_2}-\frac{\gamma_2}{\gamma_3}\right)\sin\left(\gamma_2 h_m\right)\right]},$$

$$G(\kappa,z_1) = -i\frac{\kappa\omega\left[\left(\varepsilon_0\gamma_3+\varepsilon_3\gamma_1\right)h_m\sin\left(\gamma_2 h_m\right)-\frac{1}{\gamma_2}\left(\varepsilon_0\gamma_1\gamma_3-\varepsilon_3\gamma_2^2\right)h_m\cos\left(\gamma_2 h_m\right)+\frac{1}{\gamma_2^2}\left(\varepsilon_0\gamma_1\gamma_3+\varepsilon_3\gamma_2^2\right)\sin\left(\gamma_2 h_m\right)\right]}{2c\varepsilon_0\gamma_2\gamma_3\left[\left(1+\frac{\varepsilon_3\gamma_1}{\varepsilon_1\gamma_3}\right)\cos\left(\gamma_2 h_m\right)+\left(\frac{\varepsilon_0\gamma_1}{\varepsilon_1\gamma_2}-\frac{\varepsilon_3\gamma_2}{\varepsilon_0\gamma_3}\right)\sin\left(\gamma_2 h_m\right)\right]}.$$

For arbitrary z, the relations between the field components for both quasi-TE and quasi-TM modes can be obtained by the following equations:

$$E_{2z} = \left[K_1\exp(i\gamma_a z)+K_2\exp(-i\gamma_a z)+K_3\exp(i\gamma_b z)+K_4\exp(-i\gamma_b z)\right]\exp[i(\kappa x-\omega t)],$$

$$E_{2x} = -\frac{\gamma_2}{\kappa}\left\{\left[1+\frac{g\omega\left(\kappa^2+2\gamma_2^2\right)}{2\sqrt{\varepsilon_0}\kappa\gamma_2^2 c}\right]\left[K_1\exp(i\gamma_a z)-K_2\exp(-i\gamma_a z)\right]\right.$$
$$\left.+\left[1-\frac{g\omega\left(\kappa^2+2\gamma_2^2\right)}{2\sqrt{\varepsilon_0}\kappa\gamma_2^2 c}\right]\left[K_3\exp\left(i\gamma_b z\right)-K_4\exp\left(-i\gamma_b z\right)\right]\right\}\exp\left[i(\kappa x-\omega t)\right],$$

$$E_{2y} = -i\frac{\omega\sqrt{\varepsilon_0}}{\kappa c}\left\{\left(1+\frac{g\omega}{2\sqrt{\varepsilon_0}\kappa c}\right)\left[K_1\exp(i\gamma_a z)+K_2\exp(-i\gamma_a z)\right]\right.$$
$$\left.-\left(1-\frac{g\omega}{2\sqrt{\varepsilon_0}\kappa c}\right)\left[K_3\exp(i\gamma_b z)+K_4\exp(-i\gamma_b z)\right]\right\}\exp[i(\kappa x-\omega t)],$$

$$H_{2x} = i\frac{\gamma_2\sqrt{\varepsilon_0}}{\kappa}\left\{\left(1+\frac{g\omega^3\sqrt{\varepsilon_0}}{2\kappa\gamma_2^2 c^3}\right)\left[K_1\exp\left(i\gamma_a z\right)-K_2\exp\left(-i\gamma_a z\right)\right]\right.$$
$$\left.-\left(1-\frac{g\omega^3\sqrt{\varepsilon_0}}{2\kappa\gamma_2^2 c^3}\right)\left[K_3\exp\left(i\gamma_b z\right)-K_4\exp\left(-i\gamma_b z\right)\right]\right\}\exp\left[i(\kappa x-\omega t)\right],$$

$$H_{2y} = -\frac{\omega\varepsilon_0}{\kappa c}\left\{\left(1+\frac{g\omega}{\sqrt{\varepsilon_0}\kappa c}\right)\left[K_1\exp\left(i\gamma_a z\right)+K_2\exp\left(-i\gamma_a z\right)\right]\right.$$
$$\left.+\left(1-\frac{g\omega}{\sqrt{\varepsilon_0}\kappa c}\right)\left[K_3\exp\left(i\gamma_b z\right)+K_4\exp\left(-i\gamma_b z\right)\right]\right\}\exp[i(\kappa x-\omega t)],$$
$$H_{2z} = -i\sqrt{\varepsilon_0}\left\{\left(1+\frac{g\omega}{2\sqrt{\varepsilon_0}\kappa c}\right)\left[K_1\exp\left(i\gamma_a z\right)+K_2\exp\left(-i\gamma_a z\right)\right]\right.$$
$$\left.-\left(1-\frac{g\omega}{2\sqrt{\varepsilon_0}\kappa c}\right)\left[K_3\exp\left(i\gamma_b z\right)+K_4\exp\left(-i\gamma_b z\right)\right]\right\}\exp\left[i(\kappa x-\omega t)\right],$$

where

$$K_1 = \left\{\frac{\kappa\gamma_1 c}{4\gamma_2\omega\sqrt{\varepsilon_0}}+i\frac{\kappa c}{4\omega\sqrt{\varepsilon_0}}-\frac{g}{\varepsilon_0}\left[\frac{\gamma_1\left(\kappa^2+2\gamma_2^2\right)}{8\gamma_2^3}+\frac{i}{4}\right]\right\}E_y\left(z_1\right)$$
$$-\left[\frac{\kappa c}{4\omega\varepsilon_0}-i\frac{\kappa\gamma_1 c}{4\gamma_2\omega\varepsilon_1}-\frac{g}{\varepsilon_0}\left(\frac{1}{8\sqrt{\varepsilon_0}}-i\frac{\gamma_1\omega^2\sqrt{\varepsilon_0^3}}{8\gamma_2^3\varepsilon_1 c^2}\right)\right]H_y\left(z_1\right),$$
$$K_2 = -\left\{\frac{\kappa\gamma_1 c}{4\gamma_2\omega\sqrt{\varepsilon_0}}-i\frac{\kappa c}{4\omega\sqrt{\varepsilon_0}}-\frac{g}{\varepsilon_0}\left[\frac{\gamma_1\left(\kappa^2+2\gamma_2^2\right)}{8\gamma_2^3}-\frac{i}{4}\right]\right\}E_y\left(z_1\right)$$
$$-\left[\frac{\kappa c}{4\omega\varepsilon_0}+i\frac{\kappa\gamma_1 c}{4\gamma_2\omega\varepsilon_1}-\frac{g}{\varepsilon_0}\left(\frac{1}{8\sqrt{\varepsilon_0}}+i\frac{\gamma_1\omega^2\sqrt{\varepsilon_0^3}}{8\gamma_2^3\varepsilon_1 c^2}\right)\right]H_y\left(z_1\right),$$
$$K_3 = -\left\{\frac{\kappa\gamma_1 c}{4\gamma_2\omega\sqrt{\varepsilon_0}}+i\frac{\kappa c}{4\omega\sqrt{\varepsilon_0}}+\frac{g}{\varepsilon_0}\left[\frac{\gamma_1\left(\kappa^2+2\gamma_2^2\right)}{8\gamma_2^3}+\frac{i}{4}\right]\right\}E_y\left(z_1\right)$$
$$-\left[\frac{\kappa c}{4\omega\varepsilon_0}-i\frac{\kappa\gamma_1 c}{4\gamma_2\omega\varepsilon_1}+\frac{g}{\varepsilon_0}\left(\frac{1}{8\sqrt{\varepsilon_0}}-i\frac{\gamma_1\omega^2\sqrt{\varepsilon_0^3}}{8\gamma_2^3\varepsilon_1 c^2}\right)\right]H_y\left(z_1\right),$$
$$K_4 = \left\{\frac{\kappa\gamma_1 c}{4\gamma_2\omega\sqrt{\varepsilon_0}}-i\frac{\kappa c}{4\omega\sqrt{\varepsilon_0}}+\frac{g}{\varepsilon_0}\left[\frac{\gamma_1\left(\kappa^2+2\gamma_2^2\right)}{8\gamma_2^3}-\frac{i}{4}\right]\right\}E_y\left(z_1\right)$$
$$-\left[\frac{\kappa c}{4\omega\varepsilon_0}+i\frac{\kappa\gamma_1 c}{4\gamma_2\omega\varepsilon_1}+\frac{g}{\varepsilon_0}\left(\frac{1}{8\sqrt{\varepsilon_0}}+i\frac{\gamma_1\omega^2\sqrt{\varepsilon_0^3}}{8\gamma_2^3\varepsilon_1 c^2}\right)\right]H_y\left(z_1\right).$$

APPENDIX B: THE SPATIAL PARITY OF THE QUASIWAVEGUIDE MODES

We deal with a symmetric longitudinally magnetized structure [the diagonal component of the dielectric tensor $\varepsilon(x,z) = \varepsilon(-x,z)$, and the gyration $g(x) = g(-x)$] and assume that there is no dependence on y. Let us introduce the following vector:

$$\mathbf{\Psi}(x,z) = \begin{bmatrix} E_x(x,z) \\ E_y(x,z) \\ E_z(x,z) \\ H_x(x,z) \\ H_y(x,z) \\ H_z(x,z) \end{bmatrix}, \tag{B1}$$

and the following transformation operator $\hat{T}$:

$$\hat{T}\begin{bmatrix} E_x(x,z) \\ E_y(x,z) \\ E_z(x,z) \\ H_x(x,z) \\ H_y(x,z) \\ H_z(x,z) \end{bmatrix} = \begin{bmatrix} -E_x(-x,z) \\ E_y(-x,z) \\ E_z(-x,z) \\ H_x(-x,z) \\ -H_y(-x,z) \\ -H_z(-x,z) \end{bmatrix}. \tag{B2}$$

As the magnetization vector is an axial one, the structure magnetized along the x axis has inversion symmetry with respect to coordinate inversion $x \to -x$, i.e. it transforms into itself under this operation. It implies that, at the Γ point of the Brillouin zone, a mode should transform into itself (up to a phase factor) under the operation $x \to -x$. If $\mathbf{\Psi}$ is a mode field, then taking into account that $\mathbf{E}$ and $\mathbf{H}$ are polar and axial

vectors, respectively, we come to the relation

$$\hat{T}\,\Psi = \exp(i\varphi)\,\Psi. \tag{B3}$$

According to Eq. (B2), $\hat{T}^2\Psi \equiv \Psi$, hence $\varphi = 0$ or $\varphi = \pi$. Consequently, any mode has either even parity ($\hat{T}\,\Psi = \Psi$) or odd parity ($\hat{T}\,\Psi = -\Psi$).

Obviously, the modes of even parity ($\hat{T}\,\Psi = \Psi$) satisfy the relation

$$\begin{bmatrix} E_x(x,z) \\ E_y(x,z) \\ E_z(x,z) \\ H_x(x,z) \\ H_y(x,z) \\ H_z(x,z) \end{bmatrix} = \begin{bmatrix} -E_x(-x,z) \\ E_y(-x,z) \\ E_z(-x,z) \\ H_x(-x,z) \\ -H_y(-x,z) \\ -H_z(-x,z) \end{bmatrix}, \tag{B4}$$

while the modes of odd parity ($\hat{T}\,\Psi = -\Psi$) satisfy the relation

$$\begin{bmatrix} E_x(x,z) \\ E_y(x,z) \\ E_z(x,z) \\ H_x(x,z) \\ H_y(x,z) \\ H_z(x,z) \end{bmatrix} = \begin{bmatrix} E_x(-x,z) \\ -E_y(-x,z) \\ -E_z(-x,z) \\ -H_x(-x,z) \\ H_y(-x,z) \\ H_z(-x,z) \end{bmatrix}. \tag{B5}$$

Equations (B4) and (B5) fully prove the symmetry properties of the modes presented in Table I.

APPENDIX C: DETAILS ON THE $y \to -y$ TRANSFORMATION

The plasmonic crystal considered in this paper has a permittivity that does not depend on y. The magnetization $\mathbf{M}$ is directed along the x axis. Taking into account that $\mathbf{M}$ is an axial vector, we obtain that $M \to -M$ under $y \to -y$. The same is valid for the gyration vector $g \to -g$. So the structure transforms into itself with reversed magnetization.

The wave vector of the incident wave lies in the xz plane, so being a polar vector, it keeps its direction under $y \to -y$. The polarization angle ψ is defined as $\psi = \arctan[E_y(E_x^2 + E_z^2)^{-1/2}]$. As $\mathbf{E}$ is a polar vector, $E_y \to -E_y$, and therefore $\psi \to -\psi$.

Since $\mathbf{E}$ and $\mathbf{H}$ are polar and axial vectors, respectively, the vector field components are transformed in the following way:

$$\begin{bmatrix} E_x \\ E_y \\ E_z \\ H_x \\ H_y \\ H_z \end{bmatrix} \to \begin{bmatrix} E_x \\ -E_y \\ E_z \\ -H_x \\ H_y \\ -H_z \end{bmatrix}. \tag{C1}$$

In this case, as it can easily be proved, the Maxwell's equations remain invariant, taking into account that $\varepsilon \to \varepsilon$ and $g \to -g$. The reflection and transmission constants are defined only by the magnitudes of the field components and not by their signs

$$I \propto E_x^2 + E_y^2 + E_z^2. \tag{C2}$$

It follows from Eqs. (C1) and (C2) that $I \to I$.

[1] T. Baba, Nat. Photonics **2**, 465 (2008).

[2] M. Inoue, A. Khanikaev, and A. Baryshev, in *Nanoscale Magnetic Materials and Applications*, edited by J. P. Liu, E. Fullerton, O. Gutfleisch, and D. J. Sellmyer (Springer Verlag, Dordrecht, 2009) Chap. 21, p. 627.

[3] A. K. Zvezdin and V. A. Kotov, *Modern Magnetooptics and Magnetooptical Materials* (IOP Publishing, Bristol, Philadelphia, 1997).

[4] R. Carey, E. D. Isaac, and B. W. J. Thomas, J. Phys. D **1**, 945 (1968).

[5] G. S. Krinchik and V. A. Artemjev, J. Appl. Phys. **39**, 1276 (1968).

[6] G. S. Krinchik and E. A. Ganshina, Sov. Phys. JETP **38**, 983 (1973).

[7] C. N. Afonsot and F. Briones, J. Phys. F **10**, 1253 (1980).

[8] R. Carey, B. W. J. Thomas, I. V. F. Viney, and G. H. Weaver, J. Phys. D **1**, 1679 (1968).

[9] R. R. Birss, N. Collings, and M. R. Parker, Phys. Lett. A **51**, 13 (1975).

[10] C. N. Afonso, F. Briones, and J. L. Vicent, J. Phys. D **10**, 753 (1977).

[11] G. A. Bolotin, Fiz. Met. Metalloved. **39**, 731 (1975).

[12] G. S. Krinchik and V. S. Gushchin, JETP Lett. **10**, 24 (1969).

[13] B. Donovan and T. Medcalf, Proc. Phys. Soc. **86**, 1179 (1965).

[14] G. S. Krinchik, E. A. Gan'shina, and V. S. Gushchin, Sov. Phys. JETP **33**, 115 (1971).

[15] G. Hepner and B. Désormière, Appl. Opt. **13**, 2007 (1974).

[16] T. Utikal, T. Zentgraf, S. G. Tikhodeev, M. Lippitz, and H. Giessen, Phys. Rev. B **84**, 075101 (2011).

[17] V. I. Belotelov, I. A. Akimov, M. Pohl, V. A. Kotov, S. Kasture, A. S. Vengurlekar, Achanta Venu Gopal, D. R. Yakovlev, A. K. Zvezdin, and M. Bayer, Nat. Nanotechnol. **6**, 370 (2011).

[18] V. I. Belotelov, D. A. Bykov, L. L. Doskolovich, A. N. Kalish, and A .K. Zvezdin, J. Exp. Theor. Phys. **110**, 816 (2010).

[19] V. I. Belotelov and A. K. Zvezdin, J. Magn. Magn. Mater. **300**, e260 (2006).

[20] J. F. Torrado, J. B. González-Díaz, G. Armelles, A. García-Martín, A. Altube, M. López-García, J. F. Galisteo-López, A. Blanco, and C. López, Appl. Phys. Lett. **99**, 193109 (2011).

[21] A. A. Zharov and V. V. Kurin, J. Appl. Phys. **102**, 123514 (2007).

[22] C. Clavero, K. Yang, J. R. Skuza, and R. A. Lukaszew, Opt. Lett. **35**, 1557 (2010).

[23] D. M. Newman, M. L. Wears, R. J. Matelon, and I. R. Hooper, J. Phys.: Condens. Matter **20**, 345230 (2008).

[24] S. Tkachuk, G. Lang, C. Krafft, O. Rabin, and I. Mayergoyz, J. Appl. Phys. **109**, 07B717 (2011).

[25] R. Fujikawa, A. V. Baryshev, J. Kim, H. Uchida, and M. Inoue, J. Appl. Phys. **103**, 07D301 (2008).

[26] V. Bonanni, S. Bonetti, T. Pakizeh, Z. Pirzadeh, J. Chen, J. Nogués, P. Vavassori, R. Hillenbrand, J. Åkerman, and A. Dmitriev, Nano Lett. **11**, 5333 (2011).
[27] J. C. Banthi, D. Meneses-Rodríguez, F. García, M. U. González, A. García-Martín, A. Cebollada, and G. Armelles, Adv. Mater. **24**, OP36 (2012).
[28] J. B. González-Díaz, A. García-Martín, J. M. García-Martín, A. Cebollada, G. Armelles, B. Sepúlveda, Y. Alaverdyan, and M. Käll, Small **4**, 202 (2008).
[29] M. Barthelemy and D. J. Bergman, Phys. Rev. B **58**, 12770 (1998).
[30] D. J. Bergman and Y. M. Strelniker, Phys. Rev. Lett. **80**, 857 (1998).
[31] Y. M. Strelniker and D. J. Bergman, Phys. Rev. B **59**, R12763 (1999).
[32] Y. M. Strelniker and D. J. Bergman, Phys. Rev. B **77**, 205113 (2008).
[33] A. V. Chetvertukhin, A. A. Grunin, A. V. Baryshev, T. V. Dolgova, H. Uchida, M. Inoue, and A. A. Fedyanin, J. Magn. Magn. Mater. **324**, 3516 (2012).
[34] A. A. Grunin, A. G. Zhdanov, A. A. Ezhov, E. A. Ganshina, and A. A. Fedyanin, Appl. Phys. Lett. **97**, 261908 (2010).
[35] M. Pohl, L. E. Kreilkamp, V. I. Belotelov, I. A. Akimov, A. N. Kalish, N. E. Khokhlov, V. J. Yallapragada, A. V. Gopal, M. Nur-E-Alam, M. Vasiliev, D. R. Yakovlev, K. Alameh, A. K. Zvezdin, and M. Bayer, New J. Phys. **15**, 075024 (2013).
[36] M. V. Sapozhnikov, S. A. Gusev, B. B. Troitskii, and L. V. Khokhlova, Opt. Lett. **36**, 4197 (2011).
[37] N. Kostylev, I. S. Maksymov, A. O. Adeyeye, S. Samarin, M. Kostylev, and J. F. Williams, Appl. Phys. Lett. **102**, 121907 (2013).
[38] V. I. Belotelov, A. N. Kalish, and A. K. Zvezdin, in *Magnetophotonics From Theory to Applications*, edited by M. Inoue, M. Levy, and A. V. Baryshev (Springer-Verlag, Berlin, Heidelberg, 2013) Vol. 178, Chap. 5, p. 51.
[39] I. A. Akimov, V. I. Belotelov, A. V. Scherbakov, M. Pohl, A. N. Kalish, A. S. Salasyuk, M. Bombeck, C. Brüggemann, A. V. Akimov, R. I. Dzhioev, V. L. Korenev, Yu. G. Kusrayev, V. F. Sapega, V. A. Kotov, D. R. Yakovlev, A. K. Zvezdin, and M. Bayer, J. Opt. Soc. Am. B **29**, A103 (2012).
[40] L. E. Kreilkamp, V. I. Belotelov, J. Y. Chin, S. Neutzner, D. Dregely, T. Wehlus, I. A. Akimov, M. Bayer, B. Stritzker, and H. Giessen, Phys. Rev. X **3**, 041019 (2013).
[41] B. Bai, J. Tervo, and J. Turunen, New J. Phys. **8**, 205 (2006).
[42] V. I. Belotelov, D. A. Bykov, L. L. Doskolovich, A. N. Kalish, V. A. Kotov, and A. K. Zvezdin, Opt. Lett. **34**, 398 (2009).
[43] K. Fang, Z. Yu, V. Liu, and S. Fan, Opt. Lett. **36**, 4254 (2011).
[44] V. I. Belotelov, L. L. Doskolovich, and A. K. Zvezdin, Phys. Rev. Lett. **98**, 077401 (2007).
[45] J. Y. Chin, T. Steinle, T. Wehlus, D. Dregely, T. Weiss, V. Belotelov, B. Stritzker, and H. Giessen, Nat. Commun. **4**, 1599 (2013).
[46] V. I. Belotelov, L. E. Kreilkamp, I. A. Akimov, A. N. Kalish, D. A. Bykov, S. Kasture, V. J. Yallapragada, A. V. Gopal, A. M. Grishin, S. I. Khartsev, M. Nur-E-Alam, M. Vasiliev, L. L. Doskolovich, D. R. Yakovlev, K. Alameh, A. K. Zvezdin, and M. Bayer, Nat. Commun. **4**, 2128 (2013).
[47] B. Luk'yanchuk, N. I. Zheludev, S. A. Maier, N. J. Halas, P. Nordlander, H. Giessen, and C. T. Chong, Nat. Mater. **9**, 707 (2010).
[48] S. G. Johnson, M. Ibanescu, M. A. Skorobogatiy, O. Weisberg, J. D. Joannopoulos, and Y. Fink, Phys. Rev. E **65**, 066611 (2002).
[49] A. Christ, S. G. Tikhodeev, N. A. Gippius, J. Kuhl, and H. Giessen, Phys. Rev. Lett. **91**, 183901 (2003).
[50] S. G. Tikhodeev, A. L. Yablonskii, E. A. Muljarov, N. A. Gippius, and Teruya Ishihara, Phys. Rev. B **66**, 045102 (2002).
[51] C. Ropers, G. Stibenz, G. Steinmeyer, R. Müller, D. J. Park, K. G. Lee, J. E. Kihm, J. Kim, Q. H. Park, D. S. Kim, and C. Lienau, Appl. Phys. B: Lasers Opt. **84**, 183 (2006).
[52] M. G. Moharam, Eric B. Grann, Drew A. Pommet, and T. K. Gaylord, J. Opt. Soc. Am. A **12**, 1068 (1995).
[53] L. Li, J. Opt. A: Pure Appl. Opt. **5**, 345 (2003).
[54] N. A. Gippius, S. G. Tikhodeev, and T. Ishihara, Phys. Rev. B **72**, 045138 (2005).
[55] G. Hepner, B. Désormière, and J. P. Castéra, Appl. Opt. **14**, 1479 (1975).
[56] D. O. Dzibrou and A. M. Grishin, J. Appl. Phys. **106**, 043901 (2009).
[57] S. Kahl, S. I. Khartsev, A. M. Grishin, K. Kawano, G. Kong, R. A. Chakalov, and J. S. Abell, J. Appl. Phys. **91**, 9556 (2002).
[58] P. B. Johnson and R. W. Christy, Phys. Rev. B **6**, 4370 (1972).